Estuarine, Coastal and Shelf Science 270 (2022) 107855

Contents lists available at ScienceDirect

Estuarine, Coastal and Shelf Science

journal homepage: www.elsevier.com/locate/ecss

Monsoon-driven biogeochemical dynamics in an equatorial shelf sea: Time-series observations in the Singapore Strait

Patrick Martin [a,*], Molly A. Moynihan [a,b,1], Shuang Chen [a,2], Oon Yee Woo [a], Yongli Zhou [a,1], Robert S. Nichols [a,3], Kristy Y.W. Chang [a,4], Ashleen S.Y. Tan [a,5], Ying-Hsuan Chen [c], Haojia Ren [c], Mengli Chen [d]

[a] Asian School of the Environment, Nanyang Technological University, 639798, Singapore
[b] Earth Observatory of Singapore, Interdisciplinary Graduate School, Nanyang Technological University, 639798, Singapore
[c] Department of Geosciences, National Taiwan University, Taipei, 106, Taiwan
[d] Tropical Marine Science Institute, National University of Singapore, 119227, Singapore

ARTICLE INFO

Keywords:
Nutrient dynamics
Dissolved organic matter
Coastal biogeochemistry
Tropical peatland rivers
Southeast Asia

ABSTRACT

Coastal tropical waters are experiencing rapid increases in anthropogenic pressures, yet coastal biogeochemical dynamics in the tropics are poorly studied. We present a multi-year biogeochemical time series from the Singapore Strait in Southeast Asia's Sunda Shelf Sea. Despite being highly urbanised and a major shipping port, the strait harbours numerous biologically diverse habitats and is a valuable system for understanding how tropical marine ecosystems respond to anthropogenic pressures. We observed strong seasonality driven by the semi-annual reversal of ocean currents: dissolved inorganic nitrogen (DIN) and phosphorus varied from $\leq$0.05 μmol l^{-1} during the intermonsoons to $\geq$4 μmol l^{-1} and $\geq$0.25 μmol l^{-1}, respectively, during the southwest monsoon. $Si(OH)_4$ exceeded DIN year-round. Based on nutrient concentrations, their relationships to salinity and coloured dissolved organic matter, and the isotopic composition of NO_x^-, we infer that terrestrial input from peatlands is the main nutrient source. This input delivered dissolved organic carbon (DOC) and nitrogen, but was notably depleted in dissolved organic phosphorus. In contrast, particulate organic matter showed little seasonality, and the $\delta^{13}C$ of particulate organic carbon (−21.0 ± 1.5‰) is consistent with a primarily autochthonous origin. The seasonal pattern of the diel changes in dissolved O_2 suggests that light availability controls primary productivity more than nutrient concentrations. However, diel changes in pH were greater during the southwest monsoon, when remineralisation of terrestrial DOC lowers the seawater buffer capacity. We conclude that terrestrial input results in mesotrophic conditions, and that the strait might undergo further eutrophication if nutrient inputs increase during seasons when light availability is high. Moreover, the remineralisation of terrestrial DOC within the Sunda Shelf Sea may enhance future ocean acidification.

1. Introduction

Tropical shelf seas are ecologically and economically important, but are under increasing anthropogenic pressure from coastal development, land-use change, resource extraction, and terrestrial inputs (Jennerjahn, 2012). At the same time, our understanding of the biogeochemistry of tropical shelf seas is more limited than for higher-latitude environments, which makes it harder to predict how anthropogenic pressures will affect tropical seas (Lønborg et al., 2021b; Vieillard et al., 2020).

Tropical coastal waters are often considered nutrient-poor because shelf seas exchange large volumes of water with adjacent nutrient-poor open oceans (Brunskill, 2010). However, they also receive more than

* Corresponding author.
E-mail address: pmartin@ntu.edu.sg (P. Martin).
[1] Marine Biological Laboratory, Woods Hole, MA 02543, USA.
[2] Kenyon Pte Ltd, 509016 Singapore.
[3] DHI Water & Environment (S) Pte Ltd, 608526 Singapore.
[4] Singapore Centre for Environmental Life Sciences Engineering, Nanyang Technological University, 637551 Singapore.
[5] Surbana Jurong Pte Ltd, 150168 Singapore.

https://doi.org/10.1016/j.ecss.2022.107855
Received 22 November 2021; Received in revised form 5 April 2022; Accepted 8 April 2022
Available online 13 April 2022

half of the global river input of freshwater, nutrients, and dissolved organic matter (Dai et al., 2012; Jennerjahn, 2012; Mayorga et al., 2010). Nutrient concentrations and ratios delivered by tropical rivers can be different from temperate regions: for example, tropical rivers typically have higher dissolved silicon concentrations (Jennerjahn et al., 2006). While consistently high temperature and sunlight in the tropics allow for fast rates of uptake and biogeochemical transformation of nutrients in shelf waters, high input of sediments and dissolved organic matter in the tropics can also attenuate sunlight and potentially slow the rates of nutrient utilisation (Nittrouer et al., 1995). As anthropogenic nutrient input is projected to increase substantially within the next decades, particularly in tropical Asia (Sinha et al., 2019), it is pressing to better understand the biogeochemistry of tropical coastal waters, as well as their sensitivity to ocean acidification. Southeast Asia's Sunda Shelf Sea is one of the largest and most biodiverse shelf seas globally; however, it also has dense human populations along the coast, placing high pressure on its marine habitats (Jennerjahn, 2012; Veron et al., 2009). This is especially the case in urbanised marine ecosystems that experience high anthropogenic stress (Heery et al., 2018; Todd et al., 2019). The Sunda Shelf Sea receives substantial precipitation and river input that deliver freshwater (Lee et al., 2019), terrestrial carbon (Baum et al., 2007; Huang et al., 2017; Zhou et al., 2019), and dissolved nutrients (Baum and Rixen, 2014; Jennerjahn et al., 2004; Jiang et al., 2019). While these conditions should result in dynamic coastal biogeochemistry, comparatively little biogeochemical research has been conducted in this region to date (Partelow et al., 2018). Across the open waters of the Sunda Shelf, chlorophyll-*a* concentrations are typically $\leq$0.2 μg l^{-1} (Kartadikaria et al., 2015; Ke et al., 2014), indicative of oligotrophic waters. Closer to shore and within estuaries, significant levels of eutrophication due to nutrient input have been reported, with chlorophyll-*a* of 5–50 μg l^{-1} at some sites (Chai et al., 2021; Damar et al., 2019; Lim et al., 2018, 2021; Tomascik et al., 1994). However, very few studies have collected multi-year biogeochemical time series in Southeast Asia (Lim et al., 2015, 2018). This hampers our understanding of the drivers of coastal biogeochemistry in Southeast Asia.

Here, we present a multi-year time series from the Singapore Strait, an urbanised coastal area in the central Sunda Shelf, to examine the dynamics and drivers of nutrient biogeochemistry, and their potential impacts on planktonic productivity. This study complements our previous analyses of seawater carbonate system and bio-optical variability in the Singapore Strait, which revealed a seasonal input of terrigenous dissolved organic matter from regional peatlands (Martin et al., 2021; Zhou et al., 2021).

2. Materials and methods

2.1. Site description and study design

The Singapore Strait is situated in the central Sunda Shelf Sea at 1.2°N 103.8°E (Fig. 1) and is subject to two monsoon seasons (Mayer et al., 2018; Susanto et al., 2016; van Maren and Gerritsen, 2012). During the northeast (NE) monsoon (mid-November to March), the prevailing mean circulation carries water from the open South China Sea across the Sunda Shelf, west- and northwards through the Singapore Strait and the Malacca Strait, and southwards into the Java Sea. During the southwest (SW) monsoon (mid-May to mid-September), the circulation reverses and water flows northwards from the Java Sea towards the South China Sea, while the flow in the Malacca Strait ceases or flows weakly southwards. Flow through the Singapore Strait is then eastwards and out towards the open South China Sea. The annual mean flow follows the direction of the NE monsoon, forming the South China Sea limb of the Indonesian Throughflow. During the two intermonsoon periods (April to mid-May and mid-September to mid-November) the residual flow through the Singapore Strait stagnates. Singapore experiences rainfall year-round, but rainfall is highest during the early NE monsoon (mid-November to January) and is lowest during the late NE monsoon

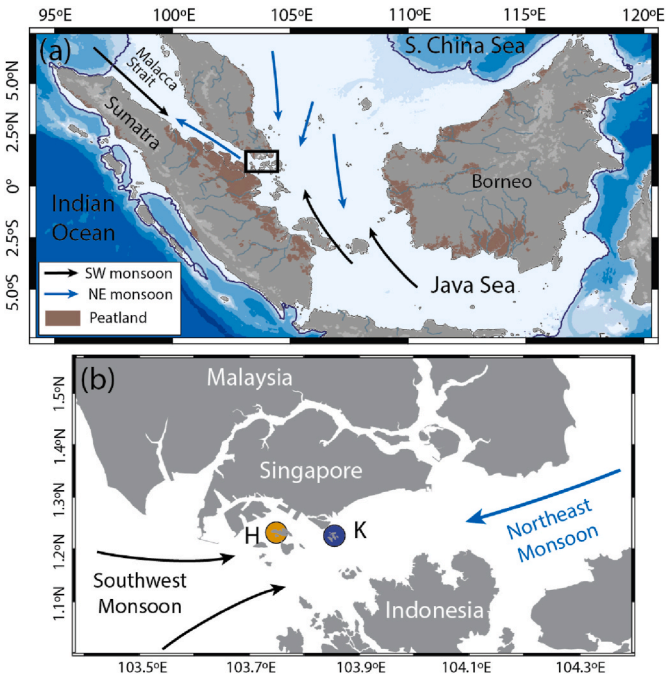

Fig. 1. Map of the study region, modified from Martin et al. (2021), indicating the seasonal current reversal between southwest (SW) and northeast (NE) monsoons (arrows) and major rivers (blue lines). Black rectangle in (a) indicates the Singapore Strait. The Sunda Shelf is delineated at the 200-m depth contour by the dark blue line. The two sampling sites, Hantu ("H") and Kusu ("K") are indicated in (b) by the two coloured dots. (For interpretation of the references to colour in this figure legend, the reader is referred to the Web version of this article.)

and early intermonsoon (February and March). Because the seawater chemistry changes considerably from early to late NE monsoon, but the late NE monsoon and first intermonsoon are very similar, we classify March as part of intermonsoon 1, as in our previous work (Martin et al., 2021; Zhou et al., 2021). We thus define the seasons as: NE monsoon = 15 Nov to end Feb; intermonsoon 1 = 01 Mar to 15 May; SW monsoon = 15 May to 15 Sept; intermonsoon 2 = 15 Sept to 15 Nov.

Because of the reversing ocean circulation, the Singapore Strait receives considerable river input from Sumatra and the western Malay Peninsula during the SW monsoon, with a notable seasonal decrease in salinity (Tanzil et al., 2019; Zhou et al., 2021) and input of terrestrial dissolved organic matter (DOM) from regional peatlands (Martin et al., 2021; Zhou et al., 2021). During the early NE monsoon, there is freshwater input from local rainfall and river flow, with a shorter period of reduced salinity and a small input of terrestrial DOM (Martin et al., 2021; Zhou et al., 2021).

Here, we present time-series data collected by regular *in-situ* water sampling at two sites in the Singapore Strait, Kusu Island (1.226°N 103.860°E) and Hantu Island (1.227°N 103.746°E) (Fig. 1). Both sites are small islands with narrow fringing reefs, with diverse communities of hard corals down to approximately 6–8 m depth (Guest et al., 2016; Huang et al., 2009). Below this depth, the seafloor consists largely of soft sediment and slopes down to 15–20 m. Sampling started in mid-2015 on an opportunistic basis for inorganic nutrients, and was carried out monthly or bi-weekly from mid-2017 for an increasing number of parameters (13–25 samples per year per site from 2018).

2.2. Sensor installation

In mid-2015, a Seabird SeaCat 19plusV2 conductivity-temperature-depth sensor (CTD) and a SeaFET pH sensor (previously Satlantic, now Seabird) were installed at ~5 m depth on the reef slope of Kusu Island,

using iron stakes such that the sensors were ~0.5 m above the seafloor. In mid-2017, a PME miniDOT dissolved oxygen (O_2) sensor was added at the same depth. The SeaFET and the miniDOT were both equipped with copper biofouling guards; the SeaCat had no antifouling protection but the pump ran during measurements to prevent sediment accumulation in the conductivity cell. All sensors measured every 10 min and were installed horizontally (except the miniDOT, which initially faced upwards but was then installed horizontally to prevent sediment accumulation on the sensor membrane). Sensors were recovered for data download and cleaning every 1–4 months. Data gaps occurred due to occasional technical problems, the need for laboratory maintenance and factory recalibration, and periods of bad data (see Section 2.5).

All salinity data are expressed on the practical salinity scale.

2.3. Water sampling

Water was collected with a Niskin bottle at 5 m depth, and a CTD profile was measured using a Valeport FastCTD with chlorophyll-*a* fluorometer. Prior to October 2017, samples were only collected for dissolved inorganic nutrient analysis, by syringe-filtering (0.2 μm Acrodisc polyethersulfone [PES] filters, 25 mm diameter) water into HCl-washed (1 M HCl here and below), 15 ml polypropylene centrifuge tubes. From October 2017, a larger number of parameters was measured, and sample water was filtered directly from the Niskin bottle with a peristaltic pump and an in-line polycarbonate filter housing (Pall, product 1119) using 0.2 μm PES membranes (47 mm diameter, Supor, Millipore). The filter, tubing, and filter housing were rinsed with 300 ml ultrapure water (18.2 MΩ cm^{-1}) and about 100 ml sample water immediately before samples were collected.

Water for $\delta^{13}C$ of dissolved inorganic carbon ($\delta^{13}C$-DIC, 1 ml) was filtered into a syringe without allowing air contact and injected into a He-flushed 12 ml Exetainer (Labco, UK) with butyl rubber septum containing 1 ml of 80% H_3PO_4. Water for DIC concentration was filled into 12 ml Exetainers, allowed to overflow, and capped with minimal headspace with a butyl rubber septum. Water for total alkalinity (TA) was filled into 125 ml high-density polyethylene (HDPE) bottles that were HCl-washed, then rinsed at least thrice with ultrapure water, dried, and rinsed twice with sample water. Water for dissolved organic carbon (DOC) and coloured dissolved organic matter (CDOM) was filled into pre-ashed (450 °C, 4 h) 40 ml amber borosilicate vials with PTFE-lined septa. Water for dissolved organic and inorganic nutrients was filled into HCl-washed 15 ml polypropylene centrifuge tubes. Water for nitrate isotopes ($\delta^{15}N$- and $\delta^{18}O$-NO_x^-) was filled into HCl-washed 125 ml HDPE bottles.

Samples for dissolved nutrients were immediately frozen in cryogenic dry shippers in the field. All other samples were stored at ambient temperature in the dark until return to the lab (within 2–5 h). All samples were then stored at +4 °C except for dissolved nutrients, $\delta^{15}N$- and $\delta^{18}O$-NO_x^- (−20 °C), and $\delta^{13}C$-DIC (room temperature). DOC samples were acidified upon collection with 100 μl 50% H_2SO_4 per 30 ml sample.

Unfiltered water was collected in the field into 1 l HCl-washed HDPE bottles to measure particulate organic carbon (POC) and particulate nitrogen (PN), particulate phosphorus (PP), $\delta^{13}C$ of POC ($\delta^{13}C$-POC), $\delta^{15}N$ of PN ($\delta^{15}N$-PN), and chlorophyll-*a*. These samples were stored at ambient temperature in the dark until returned to the laboratory, and then vacuum-filtered (0.5–1.5 l, depending on date and parameter) onto 25 mm Whatman GF/F filters (nominal pore size 0.7 μm). Except for chlorophyll-*a*, all GF/F filters were pre-ashed (450 °C 4 h), and samples were briefly rinsed with ultrapure water (~5 ml) upon filtration to prevent any carryover of dissolved nutrients. All samples were then wrapped in aluminium foil and frozen at −20 °C, except chlorophyll samples, which were flash-frozen in liquid nitrogen and stored at −80 °C.

2.4. Analyses

2.4.1. Dissolved nutrients, organic matter, and carbonate system parameters

Dissolved inorganic nutrients nitrate (NO_3^-), nitrite (NO_2^-), ammonia (NH_4^+), phosphate (PO_4^{3-}), and silicate ($Si(OH)_4$), were analysed on a SEAL AA3 segmented-flow autoanalyser. The methods for $NO_3^- + NO_2^-$, NO_2^-, PO_4^{3-}, and $Si(OH)_4$ followed the colorimetric techniques of Hansen and Koroleff (1999) according to SEAL methods G172, G173, G297, and G177. NH_4^+ was analysed fluorometrically after reaction with o-phthaldialdehyde according to SEAL method G327, based on Kérouel and Aminot (1997). Detection limits were 0.05 μmol l^{-1} ($NO_3^- + NO_2^-$), 0.01 μmol l^{-1} (NO_2^-), 0.016 μmol l^{-1} (PO_4^{3-}), 0.1 μmol l^{-1} ($Si(OH)_4$), and 0.25 μmol l^{-1} (NH_4^+).

Samples (4.5 ml) for dissolved organic nitrogen and phosphorus (DON and DOP) were oxidised in tightly capped glass centrifuge tubes with 0.5 ml of oxidative reagent (6 g $K_2S_2O_8$ with 3 g $B(OH)_3$ in 100 ml of 0.42 M NaOH) and autoclaving at 120 °C for 30 min. Samples were then diluted 1:1 with artificial seawater and analysed as for inorganic NO_3^- and PO_4^{3-}. For DOP analysis, we introduced additional ascorbic acid together with the sodium dodecyl sulphate solution via the first reagent line, such that the solution stream contained 40 mmol l^{-1} ascorbic acid before the colour reagents were introduced. This reduces interference from chlorine species generated during wet oxidation (Ma et al., 2017). Oxidation efficiency was monitored with ethylenediamine tetraacetic acid (DON) and glucose-6-phosphate (DOP), and was always ≥92%.

Dissolved organic carbon (DOC) was analysed on a Shimadzu TOC-L instrument equipped with the manufacturer's high-salt kit, calibrated with potassium hydrogen phthalate, and validated using the University of Miami deep-sea certified reference material. Coloured dissolved organic matter (CDOM) was measured on a Thermo Evolution300 dual-beam spectrophotometer against ultrapure water as the reference using 10-cm pathlength quartz cuvettes. Data were baseline-corrected (Green and Blough, 1994), smoothed using a loess function, and converted to Napierian absorption coefficients. We use the CDOM absorption coefficient at 350 nm, a_{350}, as a measure of CDOM concentration.

TA and DIC were analysed on AS-C5 and AS-ALK2 instruments (Apollo SciTech), calibrated with certified reference material from Scripps Institution of Oceanography (Batch 172) or with an in-house secondary standard from Singapore Strait seawater (see Zhou et al., 2021). Analytical precision was ±0.15% or better. TA and DIC were used to calculate seawater pH and the pH sensitivity factor Φ_D with the R package *seacarb* (Gattuso et al., 2016) on the total pH scale, using the Valeport salinity and temperature and the measured dissolved inorganic nutrient concentrations. Dissociation constants were taken from Lueker et al. (2000) for carbonic acid, from Dickson (1990) for HSO_4^-, and from Perez and Fraga (1987) for fluoride; total boron concentration followed Uppström (1974). The sensitivity factor Φ_D is the sensitivity of pH to a change in dissolved CO_2 concentration, i.e. $\frac{\partial pH}{\partial CO_2}$ (Frankignoulle, 1994). For plotting, TA and DIC were normalised to salinity 32.

2.4.2. Particulate C, N, and P

POC and PN were analysed together after acid-fuming the filters overnight in a desiccator with concentrated HCl, then drying overnight at 40 °C, and pelleting the samples in tin foil discs (Sercon, SC1032). They were then analysed at the University of Hong Kong on a Eurovector elemental analyser and Nu Instruments Perspective isotope ratio mass spectrometer (IRMS) calibrated with acetanilide standards. PP was measured by submerging filters in 3 ml of oxidative reagent (as for DOP) in tightly capped glass centrifuge tubes and autoclaving for 30 min at 120 °C. Samples were then diluted between 1:40 and 1:100 with artificial seawater and analysed as for inorganic PO_4^{3-}; the high dilution eliminates the need for additional ascorbic acid. Oxidation efficiency was monitored with glucose-6-phosphate and was always >88%.

2.4.3. Isotope analyses

Stable carbon and nitrogen isotopes of POC and PN (δ^{13}C-POC and δ^{15}N-PN) were measured with a separate set of filters from POC and PN concentration measurements, for which a larger volume of water was filtered to yield higher instrument signals. These filters were not acid-fumed, because calcifying plankton species are essentially absent (Chénard et al., 2019; Gin et al., 2003). Samples were otherwise prepared and analysed as for POC/PN, but without acetanilide concentration standards. Instead, the analysis was calibrated with isotope standards USGS40 and 41a. Analytical precision was assessed with acetanilide standard 1 from University of Indiana and was ±0.2‰ or better for δ^{13}C and δ^{15}N.

δ^{15}N- and δ^{18}O-NO_x^- were analysed on a subset of samples from Kusu in 2019–2020 in which sufficient NO_3^- was present. Analysis was performed using an IRMS after converting all NO_x^- into N_2O with the denitrifying bacterium *Pseudomonas chlororaphis* strain ATCC 13985 (Sigman et al., 2001). The standard reference materials IAEA-NO_3^- (−1.8‰ vs. air) and USGS 34 (4.7‰ vs. air) were prepared every 8–10 samples to constrain the performance of the bacterial conversion and the instrument stability. The instrument stability was further monitored by a series of prepared N_2O gas vials at the beginning and the end of each run and every 10 samples. The average standard deviation of the δ^{15}N measurements on sample replicates was less than ±0.1‰.

δ^{13}C-DIC was analysed partly at the UC Davis Stable Isotope Laboratory and partly at Nanyang Technological University using a Gas Bench connected to a Thermo Delta V IRMS, as described by Zhou et al. (2021). Analytical precision was ±0.1‰ at UC Davis and ±0.2‰ for our in-house analysis.

2.4.4. Chlorophyll-a

Chlorophyll-*a* was measured on a Horiba Fluoromax4 spectrofluorometer at excitation 436 nm and emission 680 nm (both with bandpass 5 nm) according to Welschmeyer (1994), after extracting the samples in 90% acetone at +4 °C overnight in the dark. Samples were thoroughly mixed and centrifuged at 500 rcf for 10 min prior to analysis. Calibration was performed using spinach chlorophyll-*a* (Sigma-Aldrich, C5753).

2.5. Sensor data quality control and analysis

The Valeport CTD profiles were used to calculate the mean salinity, temperature, and chlorophyll-*a* between 4.5 and 5.5 m depth to accompany our water sample data. The chlorophyll fluorometer malfunctioned and consistently returned <0.1 μg l^{-1} between October 2018 and July 2019 until it was repaired; these data were omitted.

All data from the moored sensors were checked manually to remove spikes and periods with suspect data, e.g. when heavy biofouling was noted on the sensor parts. For dates when both SeaCAT and Valeport data were available, the Valeport data were compared to the SeaCAT measurement closest in time; except for two outliers in salinity, the data agreed with root mean squared error (RMSE) of ±0.07 (salinity) and ±0.08 °C (Fig. S1).

The SeaFET pH data (total pH scale) were reprocessed based on the SeaCAT salinity; when no SeaCAT data were available, a salinity of 30 was assumed (the salinity correction is too small to impact our results significantly). Comparing the pH calculated from TA and DIC with the closest matching (within 3 h of water sampling) individual SeaFET pH measurement for all dates when good-quality SeaFET measurements were available showed that the data clustered around the 1:1 line with RMSE of 0.028 pH units across a pH range of 7.85–8.01 (Fig. S1).

Laboratory measurements of dissolved O_2 are not available for comparison to the miniDOT. Hence, the data were only examined qualitatively to remove periods where either the diel change increased considerably, or we observed a clear decrease in daily average concentration and a large increase in diel variation. This was likely caused by biofouling and/or accumulation of suspended particulates on the sensor interface, as the variability decreased after sensor cleaning. The saturated dissolved O_2 concentration was calculated following Garcia and Gordon (1992) using the SeaCAT and Valeport data.

The 10-min frequency measurements of pH and dissolved O_2 were first converted to daily anomalies by subtracting the daily mean value from the measurements on each day. The mean diel cycle was then calculated by averaging the data across all dates for every time of day. Moreover, we calculated the diel change in pH and dissolved O_2 as the maximum minus the minimum diel anomaly value on each day.

2.6. Statistical analysis and previous data use

Data were analysed and plotted in R (R Core Team, 2020). Seasonal variation was assessed using non-parametric Kruskal-Wallis tests with post-hoc Dunn tests. All averages are quoted as mean ± standard deviation unless specified otherwise.

The data for salinity, temperature, DOC, CDOM, chlorophyll-*a*, δ^{13}C-DIC, and the daily averages of seawater pH were previously used in our analyses of carbonate system (Zhou et al., 2021) and bio-optical variability (Martin et al., 2021). The data on inorganic and organic dissolved and particulate nutrients, δ^{13}C-POC, δ^{15}N-PN, δ^{15}N- and δ^{18}O-NO_x^-, dissolved O_2, and diel variability in pH are presented here for the first time.

3. Results

3.1. Hydrographic variability

Salinity and temperature typically ranged between 29–33 and 28–31 °C and showed pronounced seasonal variation, with highest values during the late NE monsoon and intermonsoon 1 (February to early May), and also during intermonsoon 2 (mid-September to mid-November) (Fig. 2). Salinity decreased to lower values and for a longer period during the SW monsoon (mid-May to mid-September) than during the early NE monsoon (mid-November to January), while temperature decreased more strongly during the NE monsoon than the SW monsoon. While temperature was essentially identical between both sites, the salinity during the SW monsoon was consistently lower at Hantu than at Kusu by 0.49 ± 0.22. We observed little vertical density variation and no clear pycnocline (Fig. S2), confirming that the water column is generally well mixed.

3.2. Dissolved inorganic nutrients

Except for NH_4^+, dissolved inorganic nutrient concentrations showed strong and statistically significant seasonal variations. Concentrations were elevated during the SW monsoon and to a lesser extent also during the early NE monsoon. During the intermonsoons, concentrations were mostly very low, often close to or below detection limits (Fig. 3; Table 1). Concentrations of $NO_3^- + NO_2^-$ reached 4–5 μmol l^{-1} during the SW monsoon, with NO_2^- typically contributing 0.5–1.0 μmol l^{-1} during this time, but NH_4^+ was only sporadically detectable (usually during the NE monsoon), with highest concentrations during 2018 (Fig. 3a–f). PO_4^{3-} showed the same pattern as $NO_3^- + NO_2^-$, with values ranging from below detection to ~0.35 μmol l^{-1} (Fig. 3g and h). $Si(OH)_4$ differed slightly from the other nutrients in never dropping below detection limits, and was >2 μmol l^{-1} in all but seven samples, reaching up to 13.8 μmol l^{-1} (Fig. 3i and j). $Si(OH)_4$ showed clearer peaks during the NE monsoon than the other nutrients.

3.3. Dissolved and particulate organic matter and stable isotope ratios

DOC showed a clear seasonal cycle with a typical peak of 80–100 μmol l^{-1} during both the SW and the NE monsoon, and lower values (usually 65–70 μmol l^{-1}) during the intermonsoons (Fig. 4a and b). DON showed less clear seasonality, ranging mostly between 4 and 12 μmol l^{-1}, but was slightly and significantly higher during the NE monsoon

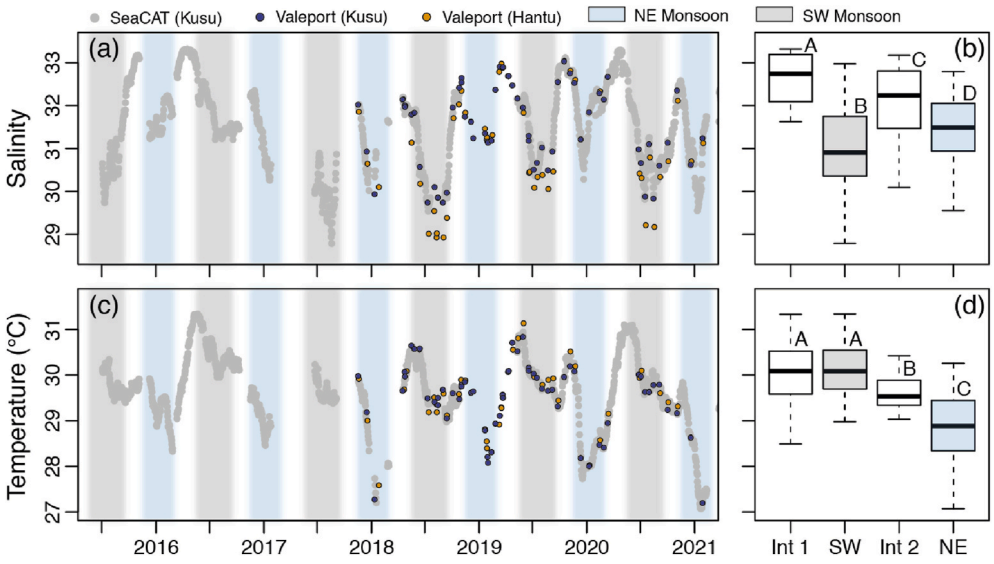

Fig. 2. Time series and seasonal boxplots of (a,b) salinity and (c,d) temperature in the Singapore Strait. Grey shading indicates the southwest (SW) monsoon, blue shading indicates the northeast (NE) monsoon. In the boxplots, Int 1 = intermonsoon 1; SW = southwest monsoon; Int 2 = intermonsoon 2; NE = northeast monsoon. Data from the Seabird SeaCAT moored CTD (at Kusu) are daily mean values; data from the Valeport FastCTD are from profiling measurements averaged at 5 m. Different letters in the boxplots indicate significant differences between seasons (Kruskal-Wallis with post-doc Dunn test, $p < 0.05$). (For interpretation of the references to colour in this figure legend, the reader is referred to the Web version of this article.)

(Fig. 4c and d). In contrast, DOP had clear seasonal variation, with very low (sometimes undetectable) concentrations during the SW monsoon and a peak of ~0.1–0.2 μmol l^{-1} during the intermonsoons and NE monsoon (Fig. 4e and f).

Unlike the dissolved nutrients, particulate matter had limited seasonal variation, with concentrations ranging mostly between 7 and 20 μmol l^{-1} for POC, 1–4 μmol l^{-1} for PN, and 0.025–0.2 μmol l^{-1} for PP (Fig. 4g–l). The concentrations were very similar between both sites, and were significantly lower during the SW monsoon and higher during either the intermonsoon or the NE monsoon periods (Fig. 4h,j,l; Table 1). The chlorophyll-*a* concentration ranged mostly between 0.5 and 2.5 μg l^{-1} with an overall mean of 1.1 ± 0.52 μg l^{-1} (Fig. 4m). Filter-based chlorophyll-*a* concentrations agreed with the Valeport FastCTD fluorometer with RMSE = 0.51 μg l^{-1} (Fig. S3). Combining the Valeport data and the filter-based data showed that chlorophyll-*a* was on average slightly but significantly elevated during intermonsoon 2 (Fig. 4n; Table 1).

δ^{13}C-POC ranged between −24.8‰ and −17.1‰, while δ^{15}N-PN ranged between +1.0‰ and +7.5‰; both showed moderate but significant differences between seasons, with lower values during the SW monsoon (Fig. 5a–d; Table 1). δ^{13}C-DIC showed an extremely clear seasonal cycle, ranging mostly from −1.5‰ to +0.5‰, with low values during the SW monsoon and high values during all other seasons (Fig. 5e and f). δ^{15}N-NO_x^- varied between +2.6‰ and +8.5‰ while δ^{18}O-NO_x^- ranged from −0.3‰ to +9.0‰ (Fig. 5g). NO_3^- concentrations were only sufficiently high during the SW and early NE monsoon to allow the isotopic composition to be measured; hence we did not test for seasonality. However, the three measurements from the NE monsoon had the lowest δ^{15}N values. There was no significant relationship between δ^{18}O-NO_x^- and δ^{15}N-NO_x^-, and the values are consistent with either marine or terrestrial NO_3^- sources (Fig. 6).

3.4. Nutrient stoichiometry and relationships between parameters

Regression statistics between parameters are given in Table 2. Dissolved inorganic nitrogen (DIN) showed a strong relationship to dissolved PO_4^{3-} that was close to the canonical Redfield ratio of 16:1, but tending towards excess PO_4^{3-} (Fig. 7a). DIN was also closely related to $Si(OH)_4$, but with a considerable excess of silicon: the DIN:$Si(OH)_4$ ratio was invariably <1, and the regression slope was 0.30 (Fig. 7b). POC and PN also showed a strong relationship that was close to the 6.6:1 Redfield stoichiometry (Fig. 7c), while PN and PP were less strongly related, with a molar N:P ratio usually above Redfield (mean of 33 ± 20; Fig. 7d). There was also no strong relationship between DOC and DON (Fig. 7e) or DON and DOP (Fig. 7f); the DOC:DON ratio was enriched in carbon relative to the Redfield value of 6.6, while the DON:DOP ratio was enriched in nitrogen relative to the Redfield value of 16 (Fig. 7e and f). Neither the POC:PN nor the PN:PP ratio showed significant seasonal variation, but both the DOC:DON and the DON:DOP ratio were significantly higher during the SW monsoon than at other times (Table 1). There was no significant relationship between POC and chlorophyll-*a* concentration, and the POC:chlorophyll-*a* ratio was relatively high, averaging 182 ± 113 g g^{-1}.

NO_3^-, PO_4^{3-}, and $Si(OH)_4$, and to a lesser degree NO_2^-, all showed strong inverse relationships with salinity (Fig. 7g–j). This was also clear for DOC, but not for DON (which peaked at intermediate salinities around 31), while DOP was positively related to salinity, but with high variability (Fig. 7k–m). POC, PN, and PP did not show significant relationships to salinity (not shown), but both δ^{13}C-POC and δ^{15}N-PN were weakly related to salinity (Fig. 7n,o). Consequently, δ^{13}C-POC and δ^{15}N-PN were also weakly related to δ^{13}C-DIC and NO_3^- concentrations, respectively (Fig. 7p,q). δ^{15}N-NO_x^- showed a clear inverse relationship to salinity and consequently a positive relationship with NO_3^- concentrations (Fig. 7r,s). Parameters that were significantly related to salinity were also significantly related to CDOM (as a_{350}), mostly with equal or slightly higher r^2 values (Fig. S4; Table S1).

3.5. Dissolved O_2 and pH dynamics

Seawater pH varied mostly between 7.80 and 8.05, showing appreciable high-frequency variability. Moreover, there was a strong seasonal difference in daily mean pH, with lowest values during the SW monsoon (Fig. 8a and b, Table 1). In contrast, dissolved O_2 showed high-frequency variability between typically 150–210 μmol l^{-1}, which was mostly below 100% saturation (Fig. 8c). Although seasonal differences in daily mean dissolved O_2 were significant, their magnitude was too small to be environmentally relevant (<5 μmol l^{-1} difference in medians; Fig. 8d, Table 1).

Plotting the daily anomalies of pH and dissolved O_2 against time revealed a clear diel cycle with a minimum at 05:30–06:30 local time and a maximum at 14:00–15:00; the average diel change was 0.022 pH units and 14.2 μmol O_2 l^{-1} (Fig. 8e and f). There was a strong relationship between the pH and dissolved O_2 anomalies at 10-min frequency (Fig. 8g), and a relationship between the diel change in pH and dissolved O_2 (Fig. 8h). The diel changes in both pH and dissolved O_2 showed significant seasonality, with diel pH change greatest during the

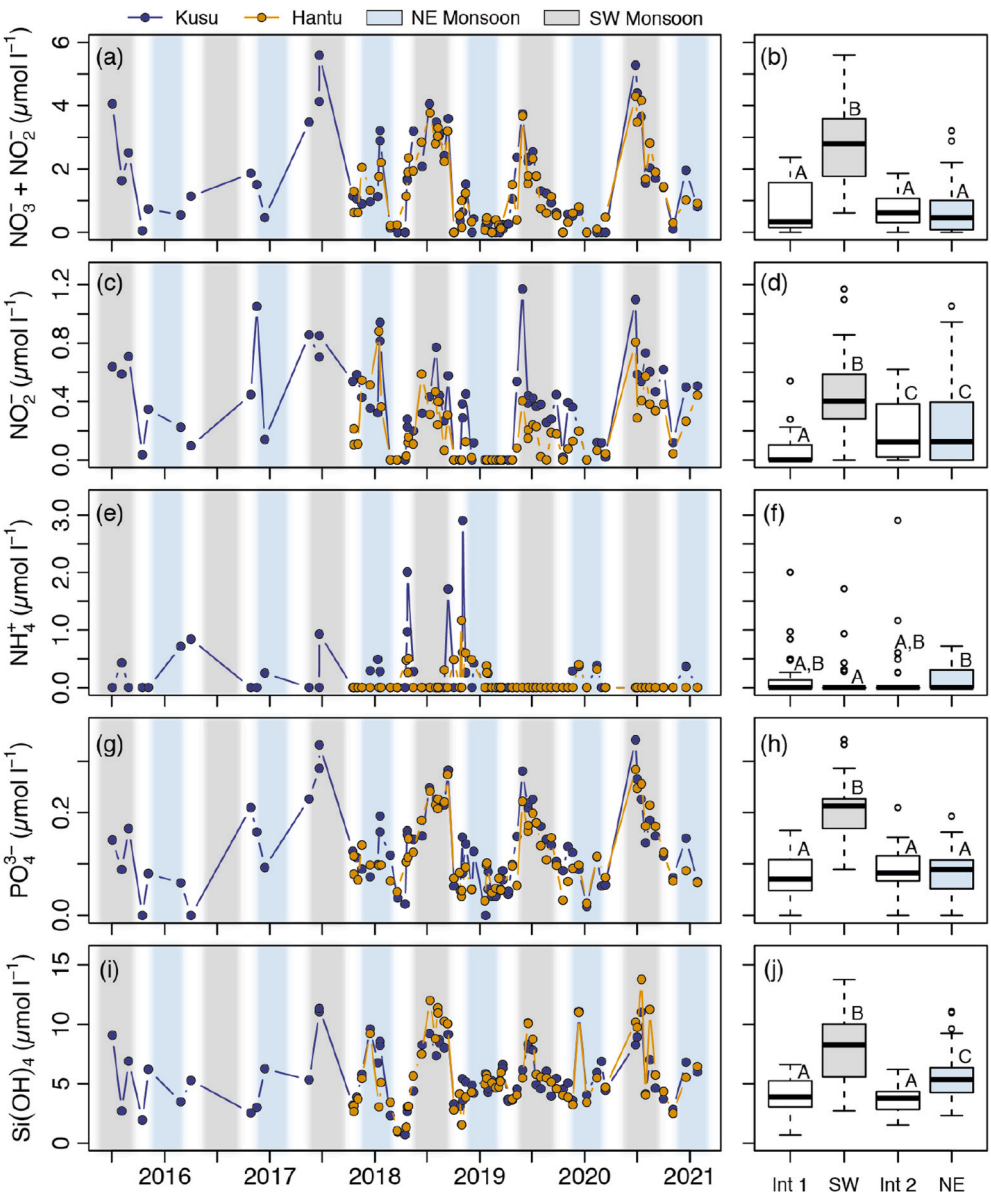

Fig. 3. Time series and seasonal boxplots of dissolved inorganic nutrient concentrations in the Singapore Strait. Colour shading and boxplot labelling are as in Fig. 2. (For interpretation of the references to colour in this figure legend, the reader is referred to the Web version of this article.)

SW and lowest during the NE monsoon, and diel dissolved O_2 change greatest during intermonsoon 1 and lowest during the NE monsoon (Fig. 8i–l, Table 1).

Salinity-normalised TA only showed a small significant decrease during intermonsoon 2 relative to other seasons (median decrease of ~20 μeq. kg^{-1}), while salinity-normalised DIC was significantly higher during the SW monsoon compared to other seasons (median increase of ~45 μmol kg^{-1}, Fig. S5). Consequently, the pH sensitivity factor Φ_D was significantly more negative during the SW monsoon (mostly between −0.0021 and −0.0024 pH units [μmol CO_2 $kg^{-1}]^{-1}$) than during other seasons (mostly between −0.0018 and −0.0020 Fig. S5).

4. Discussion

4.1. Seasonality and range in dissolved nutrient concentrations

Few studies have reported dissolved inorganic nutrient concentrations from the Singapore Strait, and existing time series are relatively short and have lower measurement frequency. Our values are broadly consistent with previous studies (Browne et al., 2015; Chénard et al., 2019; Deignan and McDougald, 2021; Gin et al., 2000), which also noted that nutrient concentrations are typically elevated during the SW monsoon. Our data clearly show that the Singapore Strait undergoes strong and consistent seasonal variation (Fig. 3): very low values (<0.5 μmol l^{-1} DIN) are seen especially during the late NE monsoon and intermonsoon 1, which are similar to reports from the open Sunda Shelf and the South China Sea (Kartadikaria et al., 2015; Liu et al., 2020; Ning et al., 2004). In contrast, nutrient concentrations during the SW monsoon are significantly elevated, and similar to values reported from the Malacca Strait (Lim et al., 2015, 2021). However, chlorophyll-*a* concentrations were above 0.4 μg l^{-1} in all but two samples, and averaged about 1 μg l^{-1} (Fig. 4), which is greater than reported from the open Sunda Shelf Sea (Kartadikaria et al., 2015; Ke et al., 2014; Liu et al., 2020). For comparison, eutrophication thresholds for coral reefs are typically considered to be ~1 μmol l^{-1} DIN, 0.1–0.2 μmol l^{-1} PO_4^{3-}, and 0.2–0.4 μg l^{-1} chlorophyll-*a* (Bell, 1992; Bell et al., 2014). This indicates that the Singapore Strait does not experience genuinely oligotrophic conditions, even when dissolved inorganic nutrients are below the

Table 1
Summary values of physical and biogeochemical properties by season. χ^2-and p-values show results of Kruskal-Wallis tests for differences between seasons (all d.f. = 3).

Parameter		Intermonsoon 1	SW monsoon	Intermonsoon 2	NE monsoon	χ^2	p
Salinity (daily mean)	Min, Max	31.63, 33.32	28.79, 32.97	30.09, 33.17	29.55, 32.79	547	<0.0001
	Mean (SD)	32.63 (0.53)	31.01 (0.85)	32.09 (0.79)	31.44 (0.70)		
	Median	32.74	30.90	32.24	31.49		
Temperature (daily mean, °C)	Min, Max	28.49, 31.33	28.98, 31.34	29.03, 30.42	27.07, 30.26	662	<0.0001
	Mean (SD)	30.06 (0.66)	30.14 (0.52)	29.64 (0.37)	28.81 (0.75)		
	Median	30.09	30.08	29.53	28.88		
pH (daily mean)	Min, Max	7.942, 7.999	7.821, 7.99	7.859, 8.033	7.865, 8.035	440	<0.0001
	Mean (SD)	7.968 (0.013)	7.896 (0.037)	7.937 (0.048)	7.980 (0.034)		
	Median	7.964	7.888	7.937	7.987		
Dissolved O_2 (daily mean; µmol l^{-1})	Min, Max	155, 193	164, 195	169, 207	155, 198	43.6	<0.0001
	Mean (SD)	181 (9.8)	178 (6.1)	184 (5.8)	180 (11.7)		
	Median	183	179	183	180		
Diel change in pH	Min, Max	0.014, 0.103	0.019, 0.1589	0.017, 0.1444	0.010, 0.162	262	<0.0001
	Mean (SD)	0.056 (0.020)	0.068 (0.023)	0.059 (0.022)	0.041 (0.019)		
	Median	0.0563	0.0662	0.0556	0.0366		
Diel change in dissolved O_2 (µmol l^{-1})	Min, Max	15.3, 78.3	13.5, 80.5	11.8, 69.5	10.0, 63.4	31.1	<0.0001
	Mean (SD)	39.5 (13.2)	35.3 (13.8)	32.8 (12.6)	28.3 (10.2)		
	Median	40.1	32.2	31.5	27.0		
$NO_3^- + NO_2^-$ (µmol l^{-1})	Min, Max	<0.05, 2.37	0.613, 5.60	<0.05, 1.86	<0.05, 3.21	71.6	<0.0001
	Mean (SD)	0.803 (0.817)	2.74 (1.16)	0.704 (0.523)	0.733 (0.816)		
	Median	0.332	2.80	0.621	0.467		
NO_2^- (µmol l^{-1})	Min, Max	<0.01, 0.538	<0.01, 1.17	<0.01, 0.620	<0.01, 1.05	42.9	<0.0001
	Mean (SD)	0.071 (0.126)	0.451 (0.251)	0.208 (0.201)	0.241 (0.292)		
	Median	<0.01	0.404	0.122	0.125		
NH_4^+ (µmol l^{-1})	Min, Max	<0.25, 2.01	<0.25, 1.72	<0.25, 2.90	<0.25, 0.719	8.78	0.032
	Mean (SD)	0.211 (0.474)	0.075 (0.285)	0.210 (0.575)	0.149 (0.200)		
	Median	<0.25	<0.25	<0.25	<0.25		
PO_4^{3-} (µmol l^{-1})	Min, Max	<0.016, 0.165	0.089, 0.342	<0.016, 0.210	<0.016, 0.193	82.3	<0.0001
	Mean (SD)	0.080 (0.045)	0.206 (0.054)	0.089 (0.041)	0.085 (0.042)		
	Median	0.071	0.213	0.083	0.090		
$Si(OH)_4$ (µmol l^{-1})	Min, Max	0.688, 6.62	2.71, 13.77	1.54, 6.20	2.32, 11.08	61.6	<0.0001
	Mean (SD)	3.89 (1.69)	7.88 (2.57)	3.70 (1.14)	5.60 (2.09)		
	Median	3.89	8.26	3.79	5.35		
POC (µmol l^{-1})	Min, Max	8.74, 19.9	6.78, 29.8	8.33, 22.3	7.84, 22.3	11.9	0.008
	Mean (SD)	13.5 (3.48)	11.7 (4.21)	14.0 (3.28)	14.2 (3.81)		
	Median	13.6	11.2	13.6	13.2		
PN (µmol l^{-1})	Min, Max	1.41, 3.63	0.97, 5.35	1.49, 3.32	1.23, 4.19	7.89	0.048
	Mean (SD)	2.39 (0.75)	2.08 (0.80)	2.46 (0.51)	2.50 (0.80)		
	Median	2.18	2.06	2.58	2.16		
PP (µmol l^{-1})	Min, Max	0.02, 0.19	0.01, 0.16	0.05, 0.20	0.05, 0.22	22.6	<0.0001
	Mean (SD)	0.08 (0.04)	0.07 (0.03)	0.10 (0.04)	0.11 (0.04)		
	Median	0.08	0.07	0.08	0.11		
δ^{13}C-POC (‰)	Min, Max	−24.8, −17.1	−24.2, −18.0	−23.2, −19.3	−22.3, −18.0	21	0.0001
	Mean (SD)	−20.9 (1.6)	−21.8 (1.4)	−21.0 (1.0)	−20.1 (1.2)		
	Median	−20.7	−21.9	−20.9	−20.3		
δ^{15}N-PN (‰)	Min, Max	1.8, 7.5	1.9, 6.3	3.8, 7.0	1.0, 6.5	14.7	0.002
	Mean (SD)	4.2 (1.3)	4.0 (1.3)	5.1 (0.7)	4.8 (1.2)		
	Median	4.2	3.8	5.1	5.2		
DOC (µmol l^{-1})	Min, Max	66.0, 85.6	65.9, 108	62.6, 77.2	55.4, 91.1	55.1	<0.0001
	Mean (SD)	74.8 (4.9)	84.6 (9.7)	69.3 (3.4)	77.9 (7.1)		
	Median	73.6	84.3	69.1	77.9		
DON (µmol l^{-1})	Min, Max	4.6, 11.7	4, 9.7	2.9, 8.9	5.9, 16.6	12.6	0.0057
	Mean (SD)	7.1 (1.7)	7.1 (1.4)	6.5 (1.5)	8.7 (2.6)		
	Median	7.1	7.2	6.6	7.8		
DOP (µmol l^{-1})	Min, Max	<0.01, 0.39	<0.01, 0.13	0.03, 0.42	<0.01, 0.5	49.8	<0.0001
	Mean (SD)	0.12 (0.08)	0.03 (0.03)	0.13 (0.10)	0.15 (0.09)		
	Median	0.12	0.02	0.11	0.14		
DOC:DON ratio (molar)	Min, Max	6.9, 17.3	7.7, 19.4	7.9, 23.5	3.8, 13	16.0	0.0011
	Mean (SD)	11.1 (2.47)	12.4 (2.70)	11.6 (4.05)	9.7 (1.98)		
	Median	10.8	12.0	10.1	10.3		
DON:DOP ratio (molar)	Min, Max	18.6, 681	38.9, 1800	18.1, 146	49.4, 98.9	26.7	<0.0001
	Mean (SD)	111 (150)	309 (366)	63.8 (42.9)	63.9 (15.2)		
	Median	59.6	155	46.3	62.1		
Chl-a (CTD and filter data; µg l^{-1})	Min, Max	0.43, 1.72	0.38, 2.55	0.56, 2.60	0.27, 2.39	9.22	0.0266
	Mean (SD)	0.89 (0.31)	0.97 (0.46)	1.42 (0.65)	1.17 (0.58)		
	Median	0.84	0.88	1.32	1.01		

eutrophication thresholds.

The dissolved organic matter pool showed a somewhat different seasonal pattern. While DOC showed similar seasonality to the inorganic nutrients, as described previously (Zhou et al., 2021), the DON concentration showed very limited seasonal changes, and the DOP concentration showed an opposite seasonal pattern, with lowest concentrations during the SW monsoon and highest during the NE and intermonsoons (Fig. 4). The DOC and DON concentrations are similar to those in other coastal locations in the tropical Indo-Pacific (Kuwahara et al., 2010; Lønborg et al., 2021a; Martin et al., 2018). The DOP concentrations in Singapore are lower than reported from the Great Barrier Reef by Lønborg et al. (2021a) (0.21 ± 0.16 µmol l^{-1}), but similar to

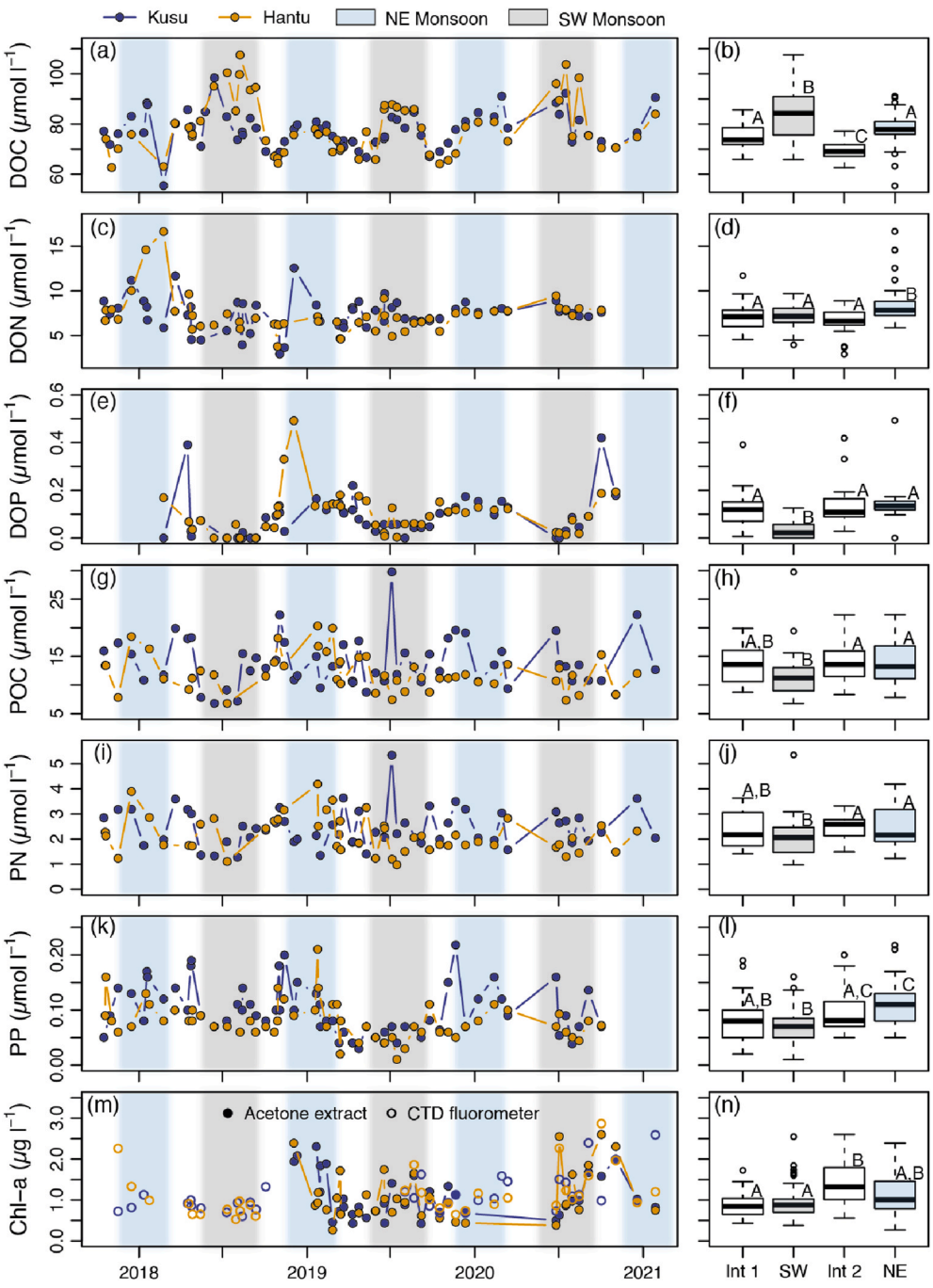

Fig. 4. Time series and seasonal boxplots of dissolved and particulate organic matter and chlorophyll-*a* concentrations. Colour shading and boxplot labelling are as for previous figures. Panel (m) shows data both from filter samples measured after acetone extraction and *in-vivo* measurements from the Valeport FastCTD fluorometer. Panel (n) includes the fluorometer data for dates when no filter-based measurements are available. (For interpretation of the references to colour in this figure legend, the reader is referred to the Web version of this article.)

recent reports from coastal locations around the Malay Peninsula (Lim et al., 2018) (0.07 ± 0.03 μmol l^{-1}). The fact that DOP was sometimes undetectable during the SW monsoon (i.e. total dissolved P was equal to dissolved PO_4^{3-}) might indicate that a refractory DOP fraction was incompletely oxidised, or alternatively that a labile DOP fraction was hydrolysed during dissolved PO_4^{3-} measurements. However, the close agreement between our two sites and consistent seasonal patterns between years clearly suggest that at least the relative variation in DOP is accurate.

Overall, and taken together with the strong seasonality in salinity (Fig. 2), our results confirm that dissolved biogeochemical properties in the Singapore Strait are largely controlled by the regional advection of distinct water masses according to the monsoon-driven changes in ocean currents, as previously described for DOC and for CDOM (Martin et al., 2021; Zhou et al., 2021). Our data also provide further support for classifying the Singapore Strait as a mesotrophic environment (Lim et al., 2021) despite the seasonally low concentrations of inorganic nutrients.

4.2. Sources of nutrients

The strong inverse relationships of NO_3^-, PO_4^{3-}, and $Si(OH)_4$ to salinity (Fig. 7) clearly indicate a terrestrial source from river input. Using stable carbon isotopes, Zhou et al. (2021) demonstrated that a large fraction of DOC in the Singapore Strait during the SW monsoon originates from surrounding peatlands. The fact that all three nutrients were more strongly correlated with CDOM than with salinity (as seen by the higher r^2 values; Fig. S4, Table S1) further supports a predominantly terrestrial source of nutrients in the Singapore Strait, as CDOM is a good tracer of terrestrial DOC in the Sunda Shelf Sea (Martin et al., 2018,

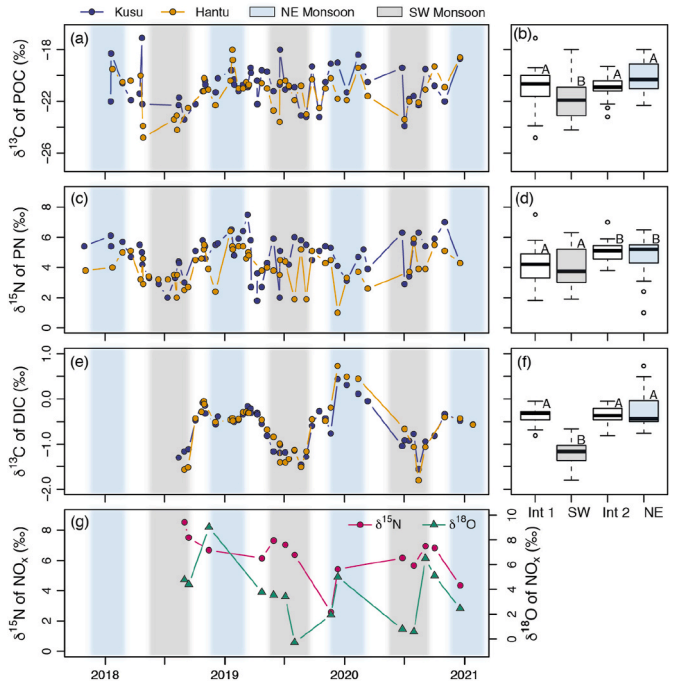

Fig. 5. Time series and seasonal boxplots of the isotopic composition ($\delta^{13}C$ and $\delta^{15}N$) of (a–d) particulate organic matter, and (e,f) dissolved inorganic carbon. Time series of $\delta^{15}N$ and $\delta^{18}O$ of NO_x^- (measured only at Kusu) is shown in (g). Since NO_x^- isotopes were only measured for dates with sufficiently high NO_3^- concentration, the seasonality was not analysed. Colour shading and boxplot labelling are as for previous figures. (For interpretation of the references to colour in this figure legend, the reader is referred to the Web version of this article.)

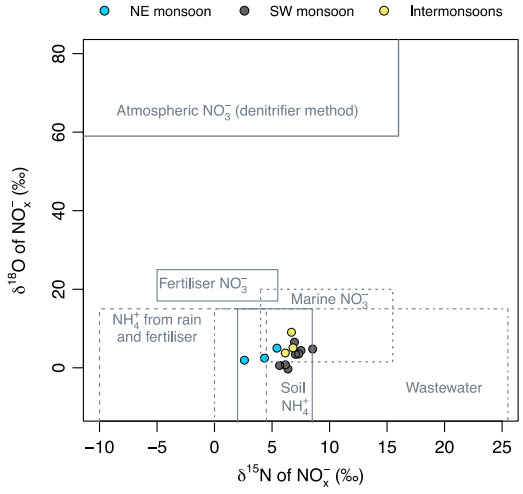

Fig. 6. Isotopic composition of dissolved NO_x^- at Kusu Island. Approximate ranges of the main potential nitrogen sources are drawn according to Kendall et al. (2007).

2021; Mizubayashi et al., 2013; Siegel et al., 2019).

The intercepts of our nutrient–salinity regressions can be taken as estimated river end-member concentrations. This implies average river concentrations of 23.7 ± 2.2 μmol l^{-1} for NO_3^-, 1.61 ± 0.14 μmol l^{-1} for PO_4^{3-}, and 59.5 ± 4.8 μmol l^{-1} for $Si(OH)_4$ (Fig. 7, Table 2). This is at the low end of $Si(OH)_4$ concentrations in small tropical rivers in Asia (Jennerjahn et al., 2006). Unpolluted tropical peatland rivers carry low nutrient concentrations, often <5 μmol l^{-1} DIN (Alkhatib et al., 2007;

Table 2
Results of linear regression analyses for relationships between key biogeochemical and physical parameters. Intercepts that are not statistically significant are marked NS. p-values refer to the significance of the regression slopes.

Parameters (y *versus* x)	Slope estimate (SE)	Intercept estimate (SE)	Statistics
DIN *versus* PO_4^{3-}	16.0 (0.77)	−0.45 (0.11)	$r^2 = 0.753$, n = 143, $p < 0.0001$
DIN *versus* $Si(OH)_4$	0.304 (0.035)	−0.16 (0.22), NS	$r^2 = 0.355$, n = 143, $p < 0.0001$
POC *versus* PN	4.69 (0.22)	2.26 (0.53)	$r^2 = 0.819$, n = 105, $p < 0.0001$
PN *versus* PP	6.03 (1.74)	1.80 (0.17)	$r^2 = 0.111$, n = 99, $p < 0.001$
NO_3^- *versus* salinity	−0.720 (0.068)	23.7 (2.16)	$r^2 = 0.461$, n = 130, $p < 0.0001$
PO_4^{3-} *versus* salinity	−0.047 (0.004)	1.61 (0.139)	$r^2 = 0.467$, n = 130, $p < 0.0001$
$Si(OH)_4$ *versus* salinity	−1.71 (0.15)	59.5 (4.80)	$r^2 = 0.494$, n = 130, $p < 0.0001$
NO_2^- *versus* salinity	−0.102 (0.020)	3.48 (0.61)	$r^2 = 0.176$, n = 130, $p < 0.0001$
DOC *versus* salinity	−6.11 (0.559)	270 (17.)	$r^2 = 0.506$, n = 119, $p < 0.0001$
DOP *versus* salinity	0.0358 (0.007)	−1.034 (0.221)	$r^2 = 0.214$, n = 98, $p < 0.0001$
$\delta^{13}C$-POC *versus* salinity	0.432 (0.132)	−34.6 (4.15)	$r^2 = 0.102$, n = 96, $p < 0.01$
$\delta^{15}N$-PN *versus* salinity	0.336 (0.112)	−6.12 (3.53), NS	$r^2 = 0.081$, n = 103, $p < 0.01$
$\delta^{15}N$-NO_x^- *versus* salinity	−0.961 (0.422)	36.1 (13.1)	$r^2 = 0.302$, n = 14, $p < 0.05$
pH anomaly *versus* dissolved O_2 anomaly (10-min frequency)	1.705×10^{-3} (7.95×10^{-6})	-1.883×10^{-5} (5.606×10^{-5}), NS	$r^2 = 0.653$, n = 24389, $p < 0.0001$
Diel pH change *versus* diel dissolved O_2 change	1.079×10^{-3} (1.25×10^{-4})	0.0288 (0.0045)	$r^2 = 0.299$, n = 179, $p < 0.0001$

Baum, 2008), because peatland ecosystems retain nutrients efficiently (Mishra et al., 2021). Although our inferred river end-member concentrations are several-fold lower than reported from highly human-impacted river systems on Java (Damar et al., 2019; Jennerjahn et al., 2004), they are well within the range reported for anthropogenically impacted peatland-draining rivers on Sumatra and Borneo (Alkhatib et al., 2007; Bange et al., 2019; Baum, 2008; Gandois et al., 2020; Jiang et al., 2019). Our data thus indicate a significant anthropogenic input of nutrients.

The fact that NO_2^- was only weakly related to salinity and CDOM (Fig. 7), while NH_4^+ was unrelated to salinity and was consistently low during the SW monsoon (Fig. 3), suggests that these two nitrogen species originate primarily from internal recycling, rather than being derived directly from land. NO_2^- and NH_4^+ concentrations in peatland rivers have only been reported from the Siak and Rajang rivers, where NO_2^- is typically <0.5 μmol l^{-1} but NH_4^+ is usually 2–15 μmol l^{-1} (Baum, 2008; Jiang et al., 2019). Our data therefore suggest that riverine NH_4^+ is rapidly transformed in the estuaries and coastal waters, likely through phytoplankton uptake and nitrification, as also reported from the Rajang delta on Borneo (Jiang et al., 2019). Recycling of organic nitrogen (either terrestrial or aquatic in origin) by ammonification followed by nitrification could also act as a source of NO_2^- in coastal waters. In subtropical coastal waters of North America, temperature-dependent NO_2^- accumulation can occur when NH_4^+ oxidation and NO_2^- oxidation become uncoupled between 20 and 30 °C, owing to the different temperature sensitivities of the microbial taxa responsible for each nitrification step (Schaefer and Hollibaugh, 2017). Whether the permanently high temperatures in tropical coastal waters might promote NO_2^- accumulation over complete nitrification may be worth testing in future research, especially in the context of increasing tropical surface temperatures. Since the water column was always oxygenated

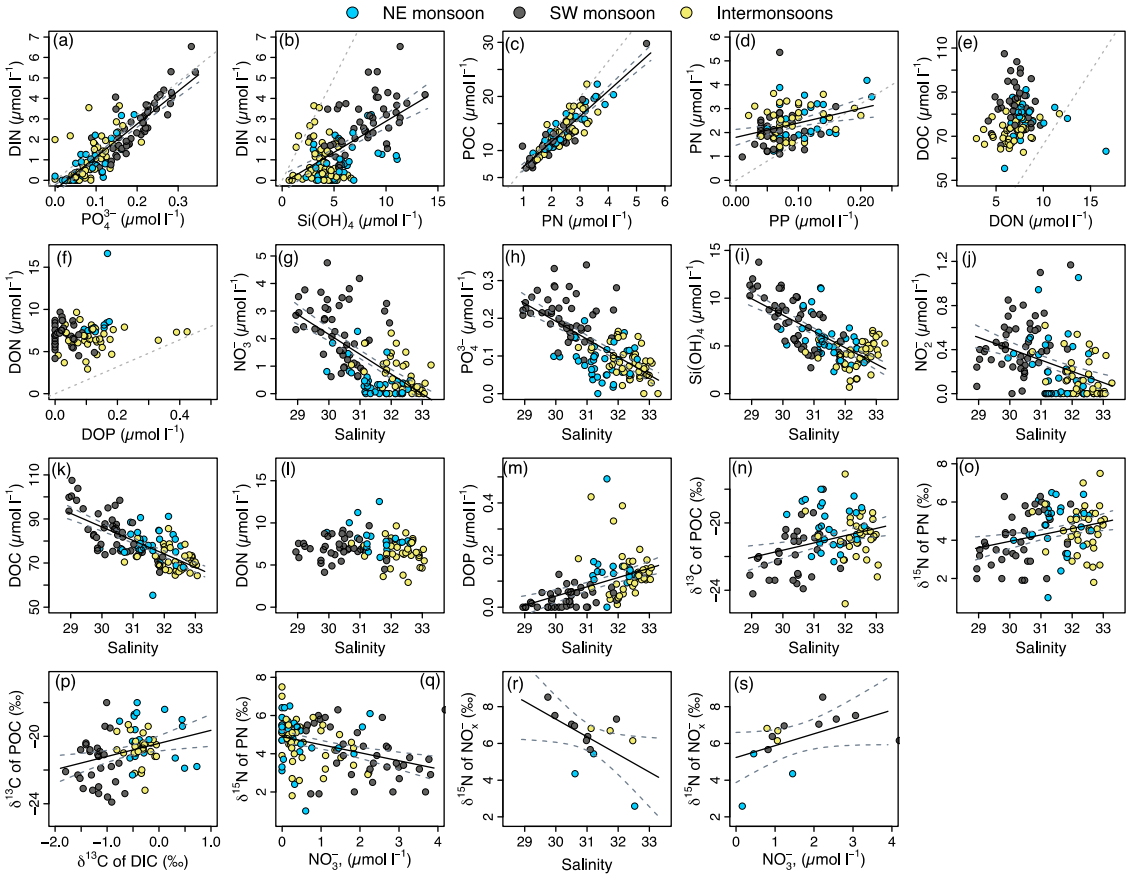

Fig. 7. Scatter plots between parameters to test for relationships and stoichiometric ratios. Solid black lines with dark-grey dashed lines indicate linear regression slopes with 95% confidence intervals; for regression parameters, see Table 2. Dotted grey lines in panels a–f indicate Redfield ratios (C:N:P = 106:16:1, N:Si = 1:1).

(Fig. 8), it is unlikely that NO_2^- accumulation was driven by hypoxia (Schaefer and Hollibaugh, 2017).

The δ^{15}N-NO_x^- and δ^{18}O-NO_x^- values are slightly higher than in the Rajang River in northwest Borneo (Jiang et al., 2019), but do not provide an unambiguous source fingerprint (Fig. 6; Kendall et al. (2007)). Although the isotopic composition could be consistent with marine NO_3^-, this is only plausible for the NE monsoon, given the strong inverse NO_3^-–salinity relationship. For the SW monsoon, the isotope data would be consistent with soil N, wastewater, or a combination of fertiliser and wastewater (Fig. 6). Most peatlands on Sumatra are used for agriculture and receive synthetic fertilisers regularly, and fertilisers and wastewater are the main nutrient sources to the Siak, which is one of the main river systems on Sumatra (Baum and Rixen, 2014). Although atmospheric deposition was suggested previously to be a significant source of NO_3^- to the Singapore Strait (Sundarambal et al., 2010), our isotope data are inconsistent with a significant atmospheric NO_3^- source. The monthly mean δ^{15}N- and δ^{18}O– NO_3^- values in rainfall in Singapore are nearly all <2‰ and >50‰, respectively (Li et al., 2020). The fact that δ^{15}N-NO_x^- during the NE monsoon had the lowest values measured, even below typical marine NO_3^- values (Fig. 6) may point to a contribution from N fixation: the shallow subsurface NO_3^- pool in the South China Sea is isotopically depleted due to diazotrophy (Ren et al., 2017; Zhang et al., 2020), and additional N fixation is likely to take place across the Sunda Shelf Sea. For example, N fixation was reported from the Singapore Strait even during the DIN-rich SW monsoon, both in the water column and associated with corals, albeit at relatively low rates (Moynihan et al., 2022).

In contrast to the main inorganic nutrients and to DOC, neither DON nor DOP appeared to have a predominant terrestrial source, given their different seasonal patterns (Fig. 4). While very low DOP concentrations during the SW monsoon might seem surprising, this provides further support for the view that peatlands are the main source of river run-off influencing the Singapore Strait during the SW monsoon (Zhou et al., 2021). Tropical peatlands are ombrotrophic, nutrient-poor systems that retain nutrients efficiently and can become particularly phosphorus-poor, while nitrogen-fixing vegetation continues to provide a nitrogen source even in old peatlands (Mishra et al., 2021; Troxler, 2007). Hence, the most likely explanation for the DON and DOP dynamics is that the DOP is predominantly of marine origin (and is hence high during the NE monsoon and intermonsoon months), while the DON has both significant marine and terrestrial sources, and hence shows little seasonality. Measurements of both DON and DOP in peatland-draining rivers would be valuable to clarify this further. While disturbed peatlands converted to agricultural use can clearly be a source of inorganic nutrients through fertiliser input, as reflected in our data, the dissolved organic matter exported from disturbed peatlands consists of increasingly old soil organic matter (Evans et al., 2014), which would explain the different dynamics of the inorganic and the organic nutrients at our site.

At present, the bioavailability of DON and DOP in the Sunda Shelf Sea is unknown. In the Great Barrier Reef, DON and DOP contributed more bioavailable N and P than either dissolved inorganic or particulate nutrients (Lønborg et al., 2018), but the DOM pool in that study was predominantly marine. In the open South China Sea, isotope data indicate active DON cycling with DON production approximately balanced by remineralisation (Zhang et al., 2020). However, peatland-derived DOC in Southeast Asia appears to be relatively refractory to direct remineralisation by heterotrophic microbes, even when inorganic N and P are added (Nichols and Martin, 2021), suggesting that the terrestrial organic nutrient pools might also be relatively refractory. Nevertheless,

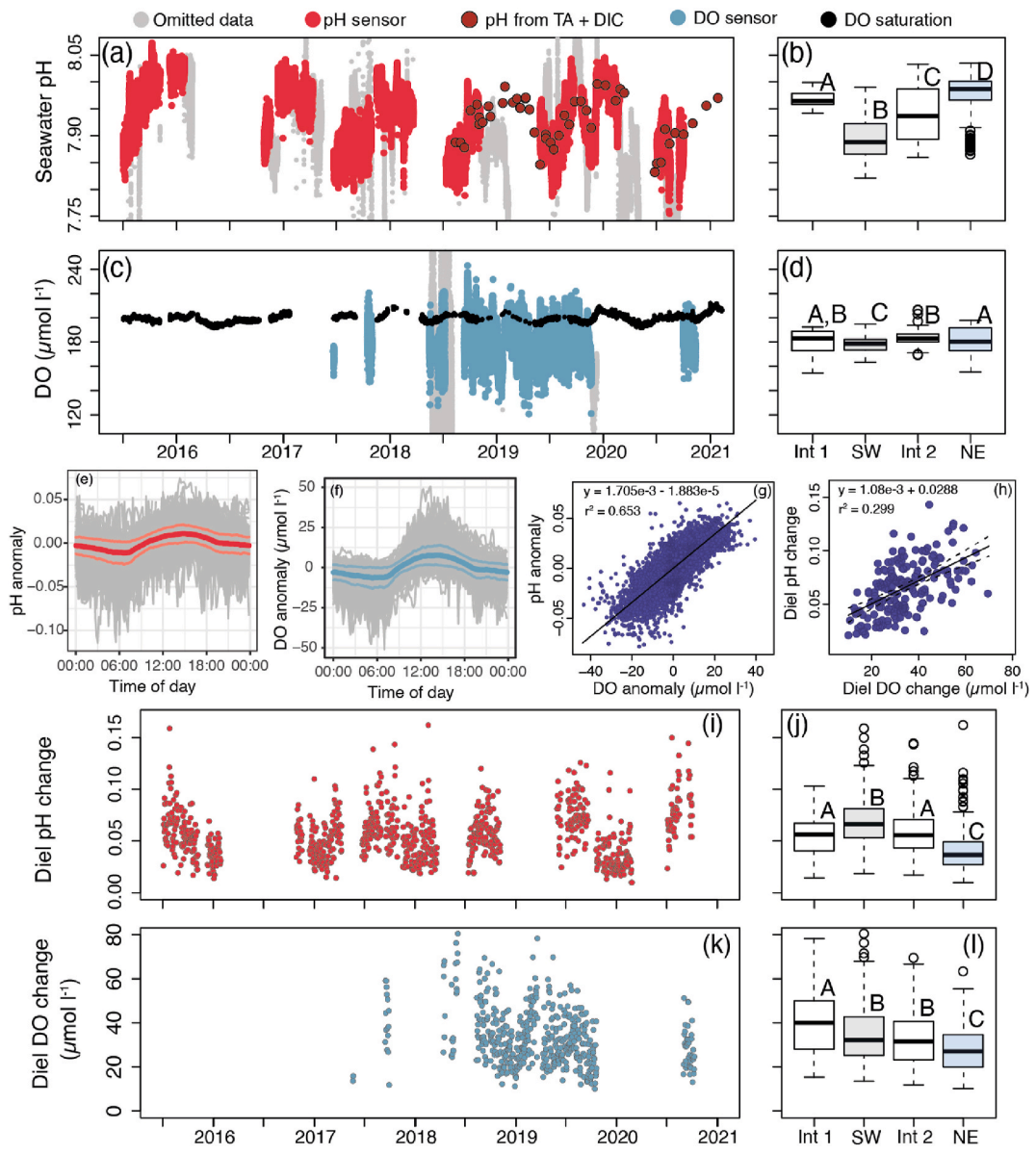

Fig. 8. Time series and seasonal boxplots of (a,b) seawater pH and (c,d) dissolved O_2 at Kusu. Black dots in panel (c) show O_2 concentration at 100% saturation. Diel anomalies of (e) seawater pH and (f) dissolved O_2; grey lines show individual daily data, solid blue and red lines show overall mean ± standard deviation. Relationships between (g) individual diel anomalies in pH and dissolved O_2 at 10-min frequency, and (h) between the maximum diel change in pH and dissolved O_2 (one point per day). Solid black and dashed grey lines indicate linear regression with 95% confidence interval. Time series and seasonal boxplots of maximum diel change in (i,j) seawater pH and (k,l) dissolved oxygen. Monsoon shading in the time series has been omitted for clarity; boxplot labelling is as for previous figures. (For interpretation of the references to colour in this figure legend, the reader is referred to the Web version of this article.)

the majority of this peatland DOC is ultimately remineralised before leaving the Sunda Shelf (Wit et al., 2018; Zhou et al., 2021), although the biogeochemical processes driving this remineralisation remain unclear. If peatland DON is also remineralised to a similar degree as DOC in the Sunda Shelf, then given the relative lack of DOP, this might lead to an imbalanced N:P ratio in areas receiving peatland run-off. Interestingly, the N:P stoichiometry of the particulate pool is typically higher than the canonical Redfield ratio of 16:1 (Fig. 7), although this might also reflect a contribution from detrital organic matter to the particulate pool (see Section 4.3). Resolving the bioavailability of the terrestrial and marine DON and DOP pools will be important for understanding the patterns of primary productivity in this region, and to reach a more complete understanding of how land use-driven changes in terrestrial DOM fluxes (Moore et al., 2013; Sanwlani et al., 2022) affect coastal seas.

4.3. Composition and dynamics of particulate organic matter

The fact that the particulate organic matter pool and the chlorophyll-*a* concentration showed only relatively limited seasonality and did not directly follow the seasonal cycle in inorganic nutrients indicates that phytoplankton biomass is not primarily controlled by nutrient availability. Even during the low-nutrient intermonsoons, chlorophyll-*a* was usually >0.5 μg l^{-1}, which suggests that nutrients are efficiently recycled during these periods to maintain phytoplankton productivity and standing stock. This is consistent with the observation of year-round measurable levels of alkaline phosphatase activity in the water column, averaging 9 nmol l^{-1} h^{-1}, most likely from heterotrophic microbial sources (Nichols, 2021). However, chlorophyll-*a* was on average elevated during intermonsoon 2 and partly also during the NE monsoon (Fig. 4). This does suggest that the SW monsoon nutrient input stimulates a delayed phytoplankton growth response. The delay might be

linked to greater light limitation during the SW monsoon due to the presence of peatland CDOM, which shoals the euphotic zone and changes the spectral quality of light underwater (Martin et al., 2021). Phytoplankton production in tropical and subtropical estuaries is similarly thought to be modulated by light limitation from high turbidity during flood events that deliver nutrients (Burford et al., 2012; Eyre, 2000), and depth-integrated phytoplankton productivity along the Great Barrier Reef is consistently greater at offshore stations with greater light availability (Furnas et al., 2005). However, the seasonal increase in chlorophyll-*a* concentration was small and not consistent between years, e.g. no increase was seen in 2019 (Fig. 4). Grazing, especially by microzooplankton, is probably also a key factor controlling phytoplankton biomass, as noted at other tropical coastal sites (Burford et al., 2008; Furnas et al., 2005; Lim et al., 2021).

Although the POC:PN ratio was very close to the Redfield ratio, the PN:PP ratio was higher (Fig. 7), and the POC:chlorophyll-*a* ratio was greater than might be expected for phytoplankton biomass in the relatively low-light environment of the Singapore Strait (Arteaga et al., 2016; Geider et al., 1997). This suggests that a significant part of the particulate organic matter pool was likely detrital. Whether this detrital fraction is primarily from marine production or from terrestrial input is unclear: the overall mean δ^{13}C-POC (-21.0 ± 1.5‰) is compatible with a purely marine origin (Fry and Sherr, 1989; Verwega et al., 2021), but the small decrease in δ^{13}C-POC might indicate a contribution of terrestrial POC during the SW monsoon (Fig. 5). However, the strong decrease in δ^{13}C-DIC during the SW monsoon, caused by peatland DOC remineralisation (Zhou et al., 2021), means that this might also reflect phytoplankton carbon assimilation from a more isotopically depleted DIC pool (Chanton and Lewis, 1999). The δ^{15}N-PN data do not help to resolve this question, as δ^{15}N-PN in Sumatran peatland rivers ranges mostly from +2‰ to +6‰ (Alkhatib et al., 2007; Baum, 2008), essentially the same as our data.

4.4. Net community metabolism

Correlations between diel changes in pH and dissolved O_2 (Fig. 8) result from planktonic and benthic community metabolism. Recent studies of coral reefs have typically focused on extensive reef flats with limited water exchange, where benthic metabolism dominates over planktonic metabolism; in such environments, coral calcification and carbonate dissolution additionally affect diel pH dynamics (Albright et al., 2015; DeCarlo et al., 2017; Page et al., 2019). Our sensors were installed along a reef slope exposed to the open sea, and the coral reef only extends about 20 m from the shoreline. Therefore, the variation in our dataset is most likely dominated just by planktonic photosynthesis and respiration.

The diel change in dissolved O_2 varied by a factor of 3–4 within each season, but was on average highest during intermonsoon 1 and lowest during the NE monsoon (Fig. 8). This pattern suggests that light availability is an important control over primary productivity: Singapore experiences lower rainfall and more solar radiation during the late NE and intermonsoon 1 than in other seasons (Fong, 2012), while CDOM input during the SW monsoon (and to a lesser degree during the early NE monsoon) increases the absorption of sunlight underwater, especially at shorter wavelengths (Martin et al., 2021). At the same time, suspended matter concentrations can vary substantially over short (<1 day) periods on reefs in Singapore (Morgan et al., 2020), further contributing to variation in light attenuation and therefore productivity rates within seasons. Seasonally-resolved measurements of primary productivity rates and diel pCO_2 dynamics would be valuable to confirm the role of light limitation in the Singapore Strait.

If phytoplankton productivity is indeed more limited by light than by nutrient availability, this would imply that increases in nutrient input might not trigger phytoplankton blooms. However, the tendency for chlorophyll-*a* to increase after the SW monsoon nutrient input (Fig. 6) suggests that phytoplankton biomass might still respond to nutrients. This could be the case especially during the low-nutrient intermonsoon periods, when CDOM concentrations are lower. Increased nutrient input, such as from future aquaculture expansion (Tan, 2020) or from greater riverine supply, might therefore still cause further eutrophication in the strait and continued monitoring is warranted. Our inorganic nutrient data suggest potential N- rather than P-limitation, but also reveal an excess of $Si(OH)_4$ over DIN (Fig. 7). This is consistent with the increase in chlorophyll-*a* observed in N-amended incubations of Singapore Strait water (Gin et al., 2006) and the large fraction of diatoms in the phytoplankton community (Chénard et al., 2019; Gin et al., 2006).

The fact that the diel change in pH does not follow the same seasonal pattern as dissolved O_2, but is on average highest during the SW monsoon (Fig. 8j), is likely driven by the greater pH sensitivity to CO_2 (Φ_D) during this season. This results from the reduced buffering capacity due to the increase in salinity-normalised DIC relative to TA (Fig. S5), which is caused by the remineralisation of peatland DOC within the Sunda Shelf (Zhou et al., 2021). Because uptake of anthropogenic CO_2 across the open South China Sea will increasingly acidify the water that enters the Sunda Shelf, the additional production of DIC from peatland DOC remineralisation within the shelf sea will further reduce the buffer capacity and enhance the ocean acidification. This is similar to the interactions between coastal carbon cycle processes and ocean acidification noted elsewhere (Cai et al., 2011; Pacella et al., 2018). Ecosystems in this part of the Sunda Shelf may therefore be particularly vulnerable to future ocean acidification, which calls for further research on the carbonate system dynamics and organismal responses to ocean acidification in this region.

5. Conclusions

Our results show that terrestrial input is a major source of dissolved inorganic nutrients to the central Sunda Shelf, with coastal waters characterised by DIN:PO_4^{3-} ratios close to the Redfield ratio, and an excess of dissolved Si over DIN. The source of nutrients is likely a combination of natural input from soils together with fertiliser and wastewater input, but atmospheric deposition appears to be at most minor. There is also a major input of peatland-derived dissolved organic matter to coastal waters, although this is notably poor in DOP. The Singapore Strait experiences strong seasonal variation because the semi-annual current reversal advects either terrestrially influenced water masses or water from the open South China Sea through the Strait. The particulate organic matter pool shows far less seasonal variation, suggesting a greater control by autochthonous marine production and possibly sediment resuspension. While there is likely a significant detrital contribution to the particulate organic matter pool, phytoplankton biomass is higher than would be expected for genuinely oligotrophic tropical waters. Phytoplankton productivity is probably limited more by light than by nutrients, but phytoplankton biomass does appear to increase in response to seasonal nutrient inputs, at least in some years. Remineralisation of terrigenous DOC lowers pH and depletes the buffering capacity on the Sunda Shelf. This *in-situ* acidification will be enhanced if the water that enters the shelf from the South China Sea has its pH and buffering capacity lowered by uptake of anthropogenic CO_2, potentially making this region of Southeast Asia more vulnerable to future ocean acidification.

Data availability

All data and analysis codes are archived in the Nanyang Technological University data repository and can be accessed at https://doi.org/10.21979/N9/2FQEGW.

CRediT authorship contribution statement

Patrick Martin: Writing – review & editing, Writing – original draft,

Visualization, Validation, Supervision, Project administration, Methodology, Investigation, Funding acquisition, Formal analysis, Data curation, Conceptualization. **Molly A. Moynihan:** Writing – review & editing, Visualization, Validation, Methodology, Investigation, Formal analysis, Data curation, Conceptualization. **Shuang Chen:** Writing – review & editing, Validation, Methodology, Investigation, Data curation. **Oon Yee Woo:** Writing – review & editing, Validation, Methodology, Investigation, Data curation. **Yongli Zhou:** Writing – review & editing, Visualization, Validation, Methodology, Investigation, Formal analysis, Data curation, Conceptualization. **Robert S. Nichols:** Writing – review & editing, Validation, Methodology, Investigation, Data curation. **Kristy Y.W. Chang:** Writing – review & editing, Validation, Methodology, Investigation, Data curation. **Ashleen S.Y. Tan:** Writing – review & editing, Validation, Methodology, Investigation, Data curation. **Ying-Hsuan Chen:** Resources, Investigation. **Haojia Ren:** Writing – review & editing, Resources, Investigation. **Mengli Chen:** Writing – review & editing, Resources, Methodology, Investigation.

Declaration of competing interest

The authors declare that they have no known competing financial interests or personal relationships that could have appeared to influence the work reported in this paper.

Acknowledgements

We are very grateful to the many colleagues and students who supported the field and laboratory work, especially Nikita Kaushal, Kyle M. Morgan, and Nathalie F. Goodkin. Francis Yeo and the crew of *Dolphin Explorer* were instrumental in supporting the field work. Isotope analysis at the University of Hong Kong was performed by Leung Kit Sum. This research was funded by the National Research Foundation, Singapore, Prime Minister's Office, through the Marine Science Research and Development Programme and the Marine Environment Sensing Network (grants MSRDP-P11, MSRDP-P32, and NRF-NRI-2020-MESN), and was carried out under research permit NP/RP17-044-3 from the Singapore National Parks Board. We thank two anonymous reviewers for constructive criticism that improved this manuscript.

Appendix A. Supplementary data

Supplementary data to this article can be found online at https://doi.org/10.1016/j.ecss.2022.107855.

References

Albright, R., Benthuysen, J., Cantin, N., Caldeira, K., Anthony, K., 2015. Coral reef metabolism and carbon chemistry dynamics of a coral reef flat. Geophys. Res. Lett. 42, 3980–3988.

Alkhatib, M., Jennerjahn, T.C., Samiaji, J., 2007. Biogeochemistry of the Dumai River estuary, Sumatra, Indonesia, a tropical black-water river. Limnol. Oceanogr. 52, 2410–2417.

Arteaga, L., Pahlow, M., Oschlies, A., 2016. Modeled Chl:C ratio and derived estimates of phytoplankton carbon biomass and its contribution to total particulate organic carbon in the global surface ocean. Global Biogeochem. Cycles 30, 1791–1810.

Bange, H.W., Sim, C.H., Bastian, D., Kallert, J., Kock, A., Mujahid, A., Müller, M., 2019. Nitrous oxide (N_2O) and methane (CH_4) in rivers and estuaries of northwestern Borneo. Biogeosciences 16, 4321–4335.

Baum, A., 2008. The Siak River in Central Sumatra, Indonesia. Ph.D. Thesis. University of Bremen.

Baum, A., Rixen, T., 2014. Dissolved inorganic nitrogen and phosphate in the human affected Blackwater river Siak, central Sumatra, Indonesia. Asian J. Water Environ. Pollut. 11, 13–24.

Baum, A., Rixen, T., Samiaji, J., 2007. Relevance of peat draining rivers in central Sumatra for the riverine input of dissolved organic carbon into the ocean. Estuar. Coast Shelf Sci. 73, 563–570.

Bell, P.R.F., 1992. Eutrophication and coral reefs—some examples in the Great Barrier Reef lagoon. Water Res. 26, 553–568.

Bell, P.R.F., Elmetri, I., Lapointe, B.E., 2014. Evidence of large-scale chronic eutrophication in the Great Barrier Reef: quantification of chlorophyll a thresholds for sustaining coral reef communities. Ambio 43, 361–376.

Browne, N.K., Tay, J.K.L., Low, J., Larson, O., Todd, P.A., 2015. Fluctuations in coral health of four common inshore reef corals in response to seasonal and anthropogenic changes in water quality. Mar. Environ. Res. 105, 39–52.

Brunskill, G.J., 2010. Tropical margins. In: Liu, K.-K., Atkinson, L., Quiñones, R., Talaue-McManus, L. (Eds.), Carbon and Nutrient Fluxes in Continental Margins: A Global Synthesis. Springer Berlin Heidelberg, Berlin, Heidelberg, pp. 423–493.

Burford, M.A., Alongi, D.M., McKinnon, A.D., Trott, L.A., 2008. Primary production and nutrients in a tropical macrotidal estuary, Darwin Harbour, Australia. Estuar. Coast Shelf Sci. 79, 440–448.

Burford, M.A., Webster, I.T., Revill, A.T., Kenyon, R.A., Whittle, M., Curwen, G., 2012. Controls on phytoplankton productivity in a wet–dry tropical estuary. Estuar. Coast Shelf Sci. 113, 141–151.

Cai, W.-J., Hu, X., Huang, W.-J., Murrell, M.C., Lehrter, J.C., Lohrenz, S.E., Chou, W.-C., Zhai, W., Hollibaugh, J.T., Wang, Y., Zhao, P., Guo, X., Gundersen, K., Dai, M., Gong, G.-C., 2011. Acidification of subsurface coastal waters enhanced by eutrophication. Nat. Geosci. 4, 766–770.

Chai, X., Li, X., Hii, K.S., Zhang, Q., Deng, Q., Wan, L., Zheng, L., Lim, P.T., Tan, S.N., Mohd-Din, M., Song, C., Song, L., Zhou, Y., Cao, X., 2021. Blooms of diatom and dinoflagellate associated with nutrient imbalance driven by cycling of nitrogen and phosphorus in anaerobic sediments in Johor Strait (Malaysia). Mar. Environ. Res. 169, 105398.

Chanton, J.P., Lewis, F.G., 1999. Plankton and dissolved inorganic carbon isotopic composition in a river-dominated estuary: Apalachicola Bay, Florida. Estuaries 22, 575–583.

Chénard, C., Wijaya, W., Vaulot, D., Lopes dos Santos, A., Martin, P., Kaur, A., Lauro, F. M., 2019. Temporal and spatial dynamics of Bacteria, Archaea and protists in equatorial coastal waters. Sci. Rep. 9, 16390.

Dai, M., Yin, Z., Meng, F., Liu, Q., Cai, W.-J., 2012. Spatial distribution of riverine DOC inputs to the ocean: an updated global synthesis. Curr. Opin. Environ. Sustain. 4, 170–178.

Damar, A., Hesse, K.-J., Colijn, F., Vitner, Y., 2019. The eutrophication states of the Indonesian sea large marine ecosystem: Jakarta Bay, 2001–2013. Deep Sea Res. II 163, 72–86.

DeCarlo, T.M., Cohen, A.L., Wong, G.T.F., Shiah, F.-K., Lentz, S.J., Davis, K.A., Shamberger, K.E.F., Lohmann, P., 2017. Community production modulates coral reef pH and the sensitivity of ecosystem calcification to ocean acidification. J. Geophys. Res. Ocean. 122, 745–761.

Deignan, L.K., McDougald, D., 2021. Differential response of the microbiome of *Pocillopora acuta* to reciprocal transplantation within Singapore. Microb. Ecol. 83, 608–618.

Dickson, A.G., 1990. Standard potential of the reaction: $AgCl(s) + 12H_2(g) = Ag(s) + HCl(aq)$, and and the standard acidity constant of the ion HSO_4^- in synthetic sea water from 273.15 to 318.15 K. J. Chem. Thermodyn. 22, 113–127.

Evans, C.D., Page, S.E., Jones, T., Moore, S., Gauci, V., Laiho, R., Hruška, J., Allott, T.E. H., Billett, M.F., Tipping, E., Freeman, C., Garnett, M.H., 2014. Contrasting vulnerability of drained tropical and high-latitude peatlands to fluvial loss of stored carbon. Global Biogeochem. Cycles 28, 1215–1234.

Eyre, B.D., 2000. Regional evaluation of nutrient transformation and phytoplankton growth in nine river-dominated sub-tropical east Australian estuaries. Mar. Ecol. Prog. Ser. 205, 61–83.

Fong, M., 2012. The Weather and Climate of Singapore. Meteorological Service Singapore, Singapore.

Frankignoulle, M., 1994. A complete set of buffer factors for acid/base CO_2 system in seawater. J. Mar. Syst. 5, 111–118.

Fry, B., Sherr, E.B., 1989. $\delta^{13}C$ measurements as indicators of carbon flow in marine and freshwater ecosystems. In: Rundel, P.W., Ehleringer, J.R., Nagy, K.A. (Eds.), Stable Isotopes in Ecological Research. Springer New York, New York, NY, pp. 196–229.

Furnas, M., Mitchell, A., Skuza, M., Brodie, J., 2005. In the other 90%: phytoplankton responses to enhanced nutrient availability in the Great Barrier Reef Lagoon. Mar. Pollut. Bull. 51, 253–265.

Gandois, L., Hoyt, A.M., Mounier, S., Le Roux, G., Harvey, C.F., Claustres, A., Nuriman, M., Anshari, G., 2020. From canals to the coast: dissolved organic matter and trace metal composition in rivers draining degraded tropical peatlands in Indonesia. Biogeosciences 17, 1897–1909.

Garcia, H.E., Gordon, L.I., 1992. Oxygen solubility in seawater: better fitting equations. Limnol. Oceanogr. 37, 1307–1312.

Gattuso, J.P., Epitalon, J.-M., Lavigne, H., 2016. Seacarb: seawater carbonate chemistry. R package version 3.1.1. https://CRAN.R-project.org/package=seacarb.

Geider, R.J., MacIntyre, H.L., Kana, T.M., 1997. Dynamic model of phytoplankton growth and acclimation: responses of the balanced growth rate and the chlorophyll a:carbon ratio to light, nutrient-limitation and temperature. Mar. Ecol. Prog. Ser. 148, 187–200.

Gin, K.Y.-H., Holmes, M.J., Zhang, S., Lin, X., 2006. Phytoplankton structure in the tropical port waters of Singapore. In: Wolanski, E. (Ed.), The Environment in Asia Pacific Harbours. Springer Netherlands, Dordrecht, pp. 347–375.

Gin, K.Y.-H., Lin, X., Zhang, S., 2000. Dynamics and size structure of phytoplankton in the coastal waters of Singapore. J. Plankton Res. 22, 1465–1484.

Gin, K.Y.H., Zhang, S., Lee, Y.K., 2003. Phytoplankton community structure in Singapore's coastal waters using HPLC pigment analysis and flow cytometry. J. Plankton Res. 25, 1507–1519.

Green, S.A., Blough, N.V., 1994. Optical absorption and fluorescence properties of chromophoric dissolved organic matter in natural waters. Limnol. Oceanogr. 39, 1903–1916.

Guest, J.R., Tun, K., Low, J., Vergés, A., Marzinelli, E.M., Campbell, A.H., Bauman, A.G., Feary, D.A., Chou, L.M., Steinberg, P.D., 2016. 27 years of benthic and coral

community dynamics on turbid, highly urbanised reefs off Singapore. Sci. Rep. 6, 36260.
Hansen, H.P., Koroleff, F., 1999. Determination of nutrients. Meth. Seawater Anal. 159–228.
Heery, E.C., Hoeksema, B.W., Browne, N.K., Reimer, J.D., Ang, P.O., Huang, D., Friess, D. A., Chou, L.M., Loke, L.H.L., Saksena-Taylor, P., Alsagoff, N., Yeemin, T., Sutthacheep, M., Vo, S.T., Bos, A.R., Gumanao, G.S., Syed Hussein, M.A., Waheed, Z., Lane, D.J.W., Johan, O., Kunzmann, A., Jompa, J., Suharsono, Taira, D., Bauman, A. G., Todd, P.A., 2018. Urban coral reefs: degradation and resilience of hard coral assemblages in coastal cities of East and Southeast Asia. Mar. Pollut. Bull. 135, 654–681.
Huang, D., Tun, K.P.P., Chou, L.M., Todd, P.A., 2009. An inventory of zooxanthellate scleractinian corals in Singapore, including 33 new records. Raffles Bull. Zool. 22, 69–80.
Huang, T.H., Chen, C.T.A., Tseng, H.C., Lou, J.Y., Wang, S.L., Yang, L., Kandasamy, S., Gao, X., Wang, J.T., Aldrian, E., Jacinto, G.S., Anshari, G.Z., Sompongchaiyakul, P., Wang, B.J., 2017. Riverine carbon fluxes to the South China Sea. J. Geophys. Res. Biogeosci. 122, 1239–1259.
Jennerjahn, T.C., 2012. Biogeochemical response of tropical coastal systems to present and past environmental change. Earth Sci. Rev. 114, 19–41.
Jennerjahn, T.C., Ittekkot, V., Klöpper, S., Adi, S., Purwo Nugroho, S., Sudiana, N., Yusmal, A., Prihartanto, Gaye-Haake, B., 2004. Biogeochemistry of a tropical river affected by human activities in its catchment: Brantas River estuary and coastal waters of Madura Strait, Java, Indonesia. Estuar. Coast Shelf Sci. 60, 503–514.
Jennerjahn, T.C., Knoppers, B.A., Souza, W.F.L., Brunskill, G.J., Silva, E.I.L., 2006. Factors controlling dissolved silica in tropical rivers. In: Ittekkot, V., Unger, D., Humborg, C., Tac An, N. (Eds.), The Silicon Cycle: Human Perturbations and Impacts on Aquatic Systems. Island Press, pp. 29–51.
Jiang, S., Müller, M., Jin, J., Wu, Y., Zhu, K., Zhang, G., Mujahid, A., Rixen, T., Muhamad, M.F., Sia, E.S.A., Jang, F.H.A., Zhang, J., 2019. Dissolved inorganic nitrogen in a tropical estuary in Malaysia: transport and transformation. Biogeosciences 16, 2821–2836.
Kartadikaria, A.R., Watanabe, A., Nadaoka, K., Adi, N.S., Prayitno, H.B., Soemorumekso, S., Muchtar, M., Triyulianti, I., Setiawan, A., Suratno, S., Khasanah, E.N., 2015. CO_2 sink/source characteristics in the tropical Indonesian seas. J. Geophys. Res. Ocean. 120, 7842–7856.
Ke, Z., Tan, Y., Ma, Y., Huang, L., Wang, S., 2014. Effects of surface current patterns on spatial variations of phytoplankton community and environmental factors in Sunda shelf. Continent. Shelf Res. 82, 119–127.
Kendall, C., Elliott, E.M., Wankel, S.D., 2007. Tracing anthropogenic inputs of nitrogen to ecosystems. Stable Isotopes Ecol. Environ. Sci. 375–449.
Kérouel, R., Aminot, A., 1997. Fluorometric determination of ammonia in sea and estuarine waters by direct segmented flow analysis. Mar. Chem. 57, 265–275.
Kuwahara, V.S., Nakajima, R., Othman, B.H.R., Kushairi, M.R.M., Toda, T., 2010. Spatial variability of UVR attenuation and bio-optical factors in shallow coral-reef waters of Malaysia. Coral Reefs 29, 693–704.
Lee, T., Fournier, S., Gordon, A.L., Sprintall, J., 2019. Maritime Continent water cycle regulates low-latitude chokepoint of global ocean circulation. Nat. Commun. 10, 2103.
Li, C., Li, S.-L., Yue, F.-J., He, S.-N., Shi, Z.-B., Di, C.-L., Liu, C.-Q., 2020. Nitrate sources and formation of rainwater constrained by dual isotopes in Southeast Asia: example from Singapore. Chemosphere 241, 125024.
Lim, J.H., Lee, C.W., Bong, C.W., 2021. Investigating factors driving phytoplankton growth and grazing loss rates in waters around Peninsular Malaysia. J. Oceanol. Limnol. 39, 148–159.
Lim, J.H., Lee, C.W., Bong, C.W., Affendi, Y.A., Hii, Y.S., Kudo, I., 2018. Distributions of particulate and dissolved phosphorus in aquatic habitats of Peninsular Malaysia. Mar. Pollut. Bull. 128, 415–427.
Lim, J.H., Lee, C.W., Kudo, I., 2015. Temporal variation of phytoplankton growth and grazing loss in the west coast of Peninsular Malaysia. Environ. Monit. Assess. 187, 246.
Liu, H., Wu, C., Xu, W., Wang, X., Thangaraj, S., Zhang, G., Zhang, X., Zhao, Y., Sun, J., 2020. Surface phytoplankton assemblages and controlling factors in the Strait of Malacca and Sunda shelf. Front. Mar. Sci. 7, 33.
Lønborg, C., Álvarez–Salgado, X.A., Duggan, S., Carreira, C., 2018. Organic matter bioavailability in tropical coastal waters: the Great Barrier Reef. Limnol. Oceanogr. 63, 1015–1035.
Lønborg, C., McKinna, L.I.W., Slivkoff, M.M., Carreira, C., 2021a. Coloured dissolved organic matter dynamics in the Great Barrier Reef. Continent. Shelf Res. 219, 104395.
Lønborg, C., Müller, M., Butler, E.C.V., Jiang, S., Ooi, S.K., Trinh, D.H., Wong, P.Y., Ali, S. M., Cui, C., Siong, W.B., Yando, E.S., Friess, D.A., Rosentreter, J.A., Eyre, B.D., Martin, P., 2021b. Nutrient cycling in tropical and temperate coastal waters: is latitude making a difference? Estuar. Coast Shelf Sci. 262, 107571.
Lueker, T.J., Dickson, A.G., Keeling, C.D., 2000. Ocean pCO_2 calculated from dissolved inorganic carbon, alkalinity, and equations for K_1 and K_2: validation based on laboratory measurements of CO_2 in gas and seawater at equilibrium. Mar. Chem. 70, 105–119.
Ma, J., Yuan, Y., Zhou, T., Yuan, D., 2017. Determination of total phosphorus in natural waters with a simple neutral digestion method using sodium persulfate. Limnol Oceanogr. Methods 15, 372–380.
Martin, P., Cherukuru, N., Tan, A.S.Y., Sanwlani, N., Mujahid, A., Müller, M., 2018. Distribution and cycling of terrigenous dissolved organic carbon in peatland-draining rivers and coastal waters of Sarawak, Borneo. Biogeosciences 15, 6847–6865.
Martin, P., Sanwlani, N., Lee, T.W.Q., Wong, J.M.C., Chang, K.Y.W., Wong, E.W.S., Liew, S.C., 2021. Dissolved organic matter from tropical peatlands reduces shelf sea light availability in the Singapore Strait, Southeast Asia. Mar. Ecol. Prog. Ser. 672, 89–109.
Mayer, B., Rixen, T., Pohlmann, T., 2018. The spatial and temporal variability of air-sea CO_2 fluxes and the effect of net coral reef calcification in the Indonesian seas: a numerical sensitivity study. Front. Mar. Sci. 5, 116.
Mayorga, E., Seitzinger, S.P., Harrison, J.A., Dumont, E., Beusen, A.H.W., Bouwman, A. F., Fekete, B.M., Kroeze, C., Van Drecht, G., 2010. Global nutrient export from WaterSheds 2 (NEWS 2): model development and implementation. Environ. Model. Software 25, 837–853.
Mishra, S., Page, S.E., Cobb, A.R., Lee, J.S.H., Jovani-Sancho, A.J., Sjögersten, S., Jaya, A., Aswandi, Wardle, D.A., 2021. Degradation of Southeast Asian tropical peatlands and integrated strategies for their better management and restoration. J. Appl. Ecol. 58, 1370–1387.
Mizubayashi, K., Kuwahara, V.S., Segaran, T.C., Zaleha, K., Effendy, A.W.M., Kushairi, M.R.M., Toda, T., 2013. Monsoon variability of ultraviolet radiation (UVR) attenuation and bio-optical factors in the Asian tropical coral-reef waters. Estuar. Coast Shelf Sci. 126, 34–43.
Moore, S., Evans, C.D., Page, S.E., Garnett, M.H., Jones, T.G., Freeman, C., Hooijer, A., Wiltshire, A.J., Limin, S.H., Gauci, V., 2013. Deep instability of deforested tropical peatlands revealed by fluvial organic carbon fluxes. Nature 493, 660–663.
Morgan, K.M., Moynihan, M.A., Sanwlani, N., Switzer, A.D., 2020. Light limitation and depth-variable sedimentation drives vertical reef compression on turbid coral reefs. Front. Mar. Sci. 7, 931.
Moynihan, M.A., Goodkin, N.F., Morgan, K.M., Kho, P.Y.Y., Lopes dos Santos, A., Lauro, F.M., Baker, D.M., Martin, P., 2022. Coral-associated nitrogen fixation rates and diazotrophic diversity on a nutrient-replete equatorial reef. ISME J. 16, 233–246.
Nichols, R.S., 2021. Pathways and Consequences of Dissolved Organic Matter Transformation in Tropical Coastal Waters. Ph.D. Thesis. Nanyang Technological University.
Nichols, R.S., Martin, P., 2021. Low biodegradability of dissolved organic matter from Southeast Asian peat-draining rivers. J. Geophys. Res. Biogeosci. 126 e2020JG006182.
Ning, X., Chai, F., Xue, H., Cai, Y., Liu, C., Shi, J., 2004. Physical-biological oceanographic coupling influencing phytoplankton and primary production in the South China Sea. J. Geophys. Res. Ocean. 109, C10005.
Nittrouer, C.A., Brunskill, G.J., Figueiredo, A.G., 1995. Importance of tropical coastal environments. Geo Mar. Lett. 15, 121–126.
Pacella, S.R., Brown, C.A., Waldbusser, G.G., Labiosa, R.G., Hales, B., 2018. Seagrass habitat metabolism increases short-term extremes and long-term offset of CO_2 under future ocean acidification. Proc. Natl. Acad. Sci. Unit. States Am. 115, 3870.
Page, H.N., Courtney, T.A., De Carlo, E.H., Howins, N.M., Koester, I., Andersson, A.J., 2019. Spatiotemporal variability in seawater carbon chemistry for a coral reef flat in Kāneʻohe Bay. Hawaiʻi. Limnol. Oceanogr. 64, 913–934.
Partelow, S., Schlüter, A., von Wehrden, H., Jänig, M., Senff, P., 2018. A sustainability agenda for tropical marine science. Conserv. Lett. 11, e12351.
Perez, F.F., Fraga, F., 1987. Association constant of fluoride and hydrogen ions in seawater. Mar. Chem. 21, 161–168.
Ren, H., Sigman, D.M., Martínez-García, A., Anderson, R.F., Chen, M.-T., Ravelo, A.C., Straub, M., Wong, G.T.F., Haug, G.H., 2017. Impact of glacial/interglacial sea level change on the ocean nitrogen cycle. Proc. Natl. Acad. Sci. Unit. States Am. 114, E6759.
Sanwlani, N., Evans, C.D., Müller, M., Cherukuru, N., Martin, P., 2022. Rising dissolved organic carbon concentrations in coastal waters of northeastern Borneo related to tropical peatland conversion. Sci. Adv. 8, eabi5688.
Schaefer, S.C., Hollibaugh, J.T., 2017. Temperature decouples ammonium and nitrite oxidation in coastal waters. Environ. Sci. Technol. 51, 3157–3164.
Siegel, H., Gerth, M., Stottmeister, I., Baum, A., Samiaji, J., 2019. Remote sensing of coastal discharge of SE Sumatra (Indonesia). In: Barale, V., Gade, M. (Eds.), Remote Sensing of the Asian Seas. Springer International Publishing, Cham, pp. 359–376.
Sigman, D.M., Casciotti, K.L., Andreani, M., Barford, C., Galanter, M., Böhlke, J.K., 2001. A bacterial method for the nitrogen isotopic analysis of nitrate in seawater and freshwater. Anal. Chem. 73, 4145–4153.
Sinha, E., Michalak, A.M., Calvin, K.V., Lawrence, P.J., 2019. Societal decisions about climate mitigation will have dramatic impacts on eutrophication in the 21st century. Nat. Commun. 10, 939.
Sundarambal, P., Tkalich, P., Balasubramanian, R., 2010. Impact of biomass burning on ocean water quality in Southeast Asia through atmospheric deposition: eutrophication modeling. Atmos. Chem. Phys. 10, 11337–11357.
Susanto, R.D., Zexun, W., Adi, T.R., Guohong, F., Bin, F., Agus, S., Teguh, A., Shujiang, L., Mukti, T., Agus, S., 2016. Oceanography surrounding Krakatau volcano in the Sunda strait, Indonesia. Oceanography 29, 264–272.
Tan, A., 2020. As Some Fish Farms in Johor Strait Near Maximum Production Levels, Authorities Eye Southern Expansion. The Straits Times, Singapore.
Tanzil, J.T.I., Goodkin, N.F., Sin, T.M., Chen, M.L., Fabbro, G.N., Boyle, E.A., Lee, A.C., Toh, K.B., 2019. Multi-colony coral skeletal Ba/Ca from Singapore's turbid urban reefs: relationship with contemporaneous in-situ seawater parameters. Geochem. Cosmochim. Acta 250, 191–208.
Team, R.C., 2020. R: A Language and Environment for Statistical Computing. R Foundation for Statistical Computing, Vienna, Austria.
Todd, P.A., Heery, E.C., Loke, L.H.L., Thurstan, R.H., Kotze, D.J., Swan, C., 2019. Towards an urban marine ecology: characterizing the drivers, patterns and processes of marine ecosystems in coastal cities. Oikos 128, 1215–1242.

Tomascik, T., Suharsono, Mah, A., 1994. Case Histories: a Historical Perspective of the Natural and Anthropogenic Impacts in the Indonesian Archipelago with a Focus on the Kepulauan Seribu, Java Sea. Colloquium on Global Aspects of Coral Reefs: Health, Hazard and History.

Troxler, T.G., 2007. Patterns of phosphorus, nitrogen and $\delta^{15}N$ along a peat development gradient in a coastal mire, Panama. J. Trop. Ecol. 23, 683–691.

Uppström, L.R., 1974. The boron/chlorinity ratio of deep-sea water from the Pacific Ocean. Deep Sea Res. Oceanogr. Abstr. 21, 161–162.

van Maren, D.S., Gerritsen, H., 2012. Residual flow and tidal asymmetry in the Singapore Strait, with implications for resuspension and residual transport of sediment. J. Geophys. Res. Ocean. 117.

Veron, J.E.N., Devantier, L.M., Turak, E., Green, A.L., Kininmonth, S., Stafford-Smith, M., Peterson, N., 2009. Delineating the coral triangle. Galaxea 11, 91–100.

Verwega, M.T., Somes, C.J., Schartau, M., Tuerena, R.E., Lorrain, A., Oschlies, A., Slawig, T., 2021. Description of a global marine particulate organic carbon-13 isotope data set. Earth Syst. Sci. Data 13, 4861–4880.

Vieillard, A.M., Newell, S.E., Thrush, S.F., 2020. Recovering from bias: a call for further study of underrepresented tropical and low-nutrient estuaries. J. Geophys. Res. Biogeosci. 125 e2020JG005766.

Welschmeyer, N.A., 1994. Fluorometric analysis of chlorophyll *a* in the presence of chlorophyll *b* and pheopigments. Limnol. Oceanogr. 39, 1985–1992.

Wit, F., Rixen, T., Baum, A., Pranowo, W.S., Hutahaean, A.A., 2018. The Invisible Carbon Footprint as a hidden impact of peatland degradation inducing marine carbonate dissolution in Sumatra, Indonesia. Sci. Rep. 8, 17403.

Zhang, R., Wang, X.T., Ren, H., Huang, J., Chen, M., Sigman, D.M., 2020. Dissolved organic nitrogen cycling in the south China sea from an isotopic perspective. Global Biogeochem. Cycles 34 e2020GB006551.

Zhou, Y., Evans, C.D., Chen, Y., Chang, K.Y.W., Martin, P., 2021. Extensive remineralization of peatland-derived dissolved organic carbon and ocean acidification in the Sunda shelf sea, Southeast Asia. J. Geophys. Res. Ocean. 126 e2021JC017292.

Zhou, Y., Martin, P., Müller, M., 2019. Composition and cycling of dissolved organic matter from tropical peatlands of coastal Sarawak, Borneo, revealed by fluorescence spectroscopy and parallel factor analysis. Biogeosciences 16, 2733–2749.